CXCR5+ T helper cells mediate protective immunity against tuberculosis

Samantha R. Slight,[1] Javier Rangel-Moreno,[2] Radha Gopal,[1] Yinyao Lin,[1] Beth A. Fallert Junecko,[3] Smriti Mehra,[4] Moises Selman,[5] Enrique Becerril-Villanueva,[6] Javier Baquera-Heredia,[7] Lenin Pavon,[6] Deepak Kaushal,[4] Todd A. Reinhart,[3] Troy D. Randall,[2] and Shabaana A. Khader[1]

[1]Department of Pediatrics, Division of Infectious Diseases, University of Pittsburgh School of Medicine, Pittsburgh, Pennsylvania, USA. [2]Department of Medicine, Division of Allergy, Immunology and Rheumatology, University of Rochester Medical Center, Rochester, New York, USA. [3]Department of Infectious Diseases and Microbiology, University of Pittsburgh, Pittsburgh, Pennsylvania, USA. [4]Divisions of Bacteriology and Parasitology, Tulane National Primate Research Center, Covington, Louisiana, USA. [5]Instituto Nacional de Enfermedades Respiratorias "Ismael Cosio Villegas," Mexico City, Mexico. [6]Department of Psychoimmunology, National Institute of Psychiatry "Ramon de la Fuente," Mexico City, Mexico. [7]Laboratory of Surgical Pathology, The American British Cowdray Medical Center, Mexico City, Mexico.

One third of the world's population is infected with *Mycobacterium tuberculosis* (*Mtb*). Although most infected people remain asymptomatic, they have a 10% lifetime risk of developing active tuberculosis (TB). Thus, the current challenge is to identify immune parameters that distinguish individuals with latent TB from those with active TB. Using human and experimental models of *Mtb* infection, we demonstrated that organized ectopic lymphoid structures containing CXCR5$^+$ T cells were present in *Mtb*-infected lungs. In addition, we found that in experimental *Mtb* infection models, the presence of CXCR5$^+$ T cells within ectopic lymphoid structures was associated with immune control. Furthermore, in a mouse model of *Mtb* infection, we showed that activated CD4$^+$CXCR5$^+$ T cells accumulated in *Mtb*-infected lungs and produced proinflammatory cytokines. Mice deficient in *Cxcr5* had increased susceptibility to TB due to defective T cell localization within the lung parenchyma. We demonstrated that CXCR5 expression in T cells mediated correct T cell localization within TB granulomas, promoted efficient macrophage activation, protected against *Mtb* infection, and facilitated lymphoid follicle formation. These data demonstrate that CD4$^+$CXCR5$^+$ T cells play a protective role in the immune response against TB and highlight their potential use for future TB vaccine design and therapy.

Introduction

Approximately 2 billion people are infected with *Mycobacterium tuberculosis* (*Mtb*), making tuberculosis (TB) one of the most prevalent infectious diseases in the world (1). Most infected people have latent TB (L-TB) and remain asymptomatic, although they have a 10% lifetime risk of developing active TB (A-TB). The biggest challenge with current TB control measures is the absence of well-defined immune correlates to distinguish individuals with L-TB from those with A-TB.

A hallmark of pulmonary TB in both humans and experimentally infected animals is the formation of granulomas that contain *Mtb*-infected macrophages (2). Granulomas are thought to be important for the proper activation of macrophages that control *Mtb* in the lung. Interestingly, granulomas have some characteristics, such as organized B cell follicles, that are reminiscent of ectopic lymphoid structures that form at sites of chronic inflammation or infection (3–5). In the lung, these tissues are known as inducible bronchus-associated lymphoid tissue (iBALT) (5, 6). The development of such lymphoid aggregates has been seen in lungs of patients with TB (3, 7) and associated with well-controlled L-TB, whereas the absence or disorganized lymphoid aggregates is associated with uncontrolled disease in A-TB patients (8). Despite this association, the molecular signals and cellular components orchestrating granuloma and iBALT organization, and the mechanisms mediating protection during TB, remain undefined.

T follicular helper (Tfh) cells are found in secondary lymphoid organs (SLOs) and are characterized by expression of CXCR5 (9), inducible co-stimulatory receptor (ICOS), programmed cell death gene–1 (PD-1) (10), and the transcription factor B cell lymphoma 6 protein (Bcl6) (11–13). Tfh cells participate in the generation of germinal centers (GCs) and are essential for proper T-B cell localization and B cell responses to T cell–dependent antigens (10, 14). Tfh cells also produce IL-21, which regulates generation of humoral responses and GC formation (15). Most studies have described a role for Tfh cells in generation of humoral immunity in the SLOs (10, 14); however, it is not known whether CXCR5-expressing CD4$^+$ T cells play a protective role in peripheral non-lymphoid organs and contribute to host immunity against infections.

The ligand for CXCR5, CXCL13, is constitutively expressed in SLOs and directs the placement of CXCR5$^+$ B cells (16) and activated CXCR5$^+$ T cells (17) into the B cell follicle. However, CXCL13 is also inducibly expressed in the murine lung following infection with *Mtb* (18–20), influenza (6), and in lipopolysaccharide-mediated lung inflammation (21). However, it is not known whether CXCR5$^+$ T cells localize within the lung in response to *Mtb* infection–induced CXCL13 or whether they play a role in organization of lymphoid structures within TB granulomas and mediate protective immunity. In addition, it is not known whether ectopic lymphoid follicles are a consequence of an effective immune response against *Mtb* infection, and whether they are necessary for immune control. In the current study, we show that CXCR5$^+$ T cells accumulate within ectopic lymphoid structures associated with TB granulomas in humans, non-human primates (NHPs), and mice. Furthermore, we show that the presence of CXCR5$^+$ T cells within organized ectopic lymphoid structures is associated with immune control in NHPs with L-TB, whereas the lack of lymphoid structures or presence of disorganized lym-

Conflict of interest: The authors have declared that no conflict of interest exists.
Citation for this article: *J Clin Invest.* 2013;123(2):712–726. doi:10.1172/JCI65728.

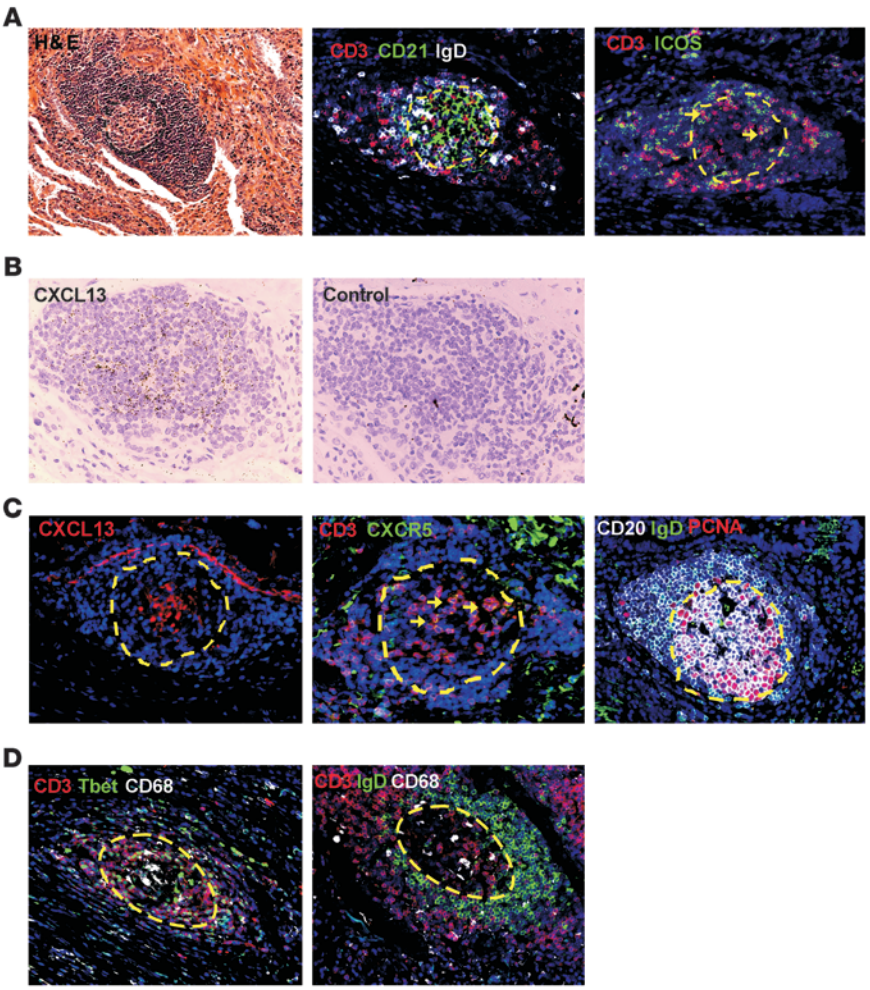

Figure 1
CXCR5$^+$ T cells accumulate within ectopic lymphoid structures of human TB granulomas. Serial sections of formalin-fixed, paraffin-embedded (FFPE) lung biopsies from A-TB patients underwent H&E staining (**A**, left panel). *CXCL13* mRNA was detected by ISH with a CXCL13 cRNA probe (**B**). Sections were analyzed by immunofluorescence using antibodies specific to CD3, CD21, IgD; and CD3, ICOS (**A**), or CXCL13; CD3, CXCR5; and PCNA, IgD, CD20 (**C**), or CD3, Tbet, CD68; and CD3, IgD, CD68 (**D**). All sections were counterstained with DAPI (blue). GC with a central core of PCNA$^+$CD20$^+$IgD$^+$ large B blasts are outlined with yellow dashed lines. Yellow arrows point to typical CD3$^+$ ICOS$^+$ or CXCR5$^+$ T cells (**A** and **C**). CXCL13 protein localizes inside a GC outlined with yellow dashed line (**C**). Original magnification, ×200; ×600 (ISH).

phoid areas is associated with active disease in NHPs. The production of proinflammatory cytokines such as IFN-γ and TNF-α is required in order to activate macrophages and mediate protective immunity against TB (22–24). Using a mouse model of *Mtb* infection in which immune control results in chronic infection, we show that activated CD4$^+$CXCR5$^+$ T cells accumulate in the *Mtb*-infected lung, express markers of Tfh-like and Th1-like cells, and co-produce proinflammatory cytokines. In addition, we show that CD4$^+$CXCR5$^+$ T cells respond to CXCL13 and localize within the lung parenchyma for efficient macrophage activation and optimal mycobacterial control. Our data also demonstrate that formation of lymphoid follicles within the granuloma requires CXCR5-dependent T cell localization, but the formation of B cell lymphoid follicles by itself is not necessary for immune control against *Mtb* infection in mice. These data together define a novel and unexpected role for CXCR5 expression on CD4$^+$ T cells in the lung to mediate control of mycobacterial infection.

Results

Ectopic lymphoid structures are associated with immune control during TB. Normal human lungs do not exhibit appreciable accumulation of lymphocytes or inflammatory aggregates (25). However, individuals with L-TB exhibit organized pulmonary lymphoid aggregates, while cellular aggregates were absent or less organized in lungs of individuals undergoing A-TB (8). We found that lung sections from 25% of A-TB patients (Supplemental Table 1; supplemental material available online with this article; doi:10.1172/JCI65728DS1) showed accumulation of lymphocytes with features of classic ectopic lymphoid structures, containing central CD21$^+$ follicular dendritic cells (FDCs) in the center of well-organized GCs that contained CD3$^+$ T cells (Figure 1A). In addition, the CD3$^+$ T cells expressed ICOS, one of the classic Tfh cell markers (Figure 1A). *CXCL13* mRNA (Figure 1B) and protein (Figure 1C) were also detected within lymphoid aggregates. Furthermore, localization of CD3$^+$ T cells expressing CXCR5 and numerous proliferating cell nuclear antigen–expressing (PCNA-expressing) CD20$^+$ B cells inside compact B cell follicles (Figure 1C) colocalized with macrophages expressing CD68 (Figure 1D), suggesting that these are bona fide ectopic lymphoid structures.

Since ectopic lymphoid structures were seen only in a minority of human A-TB granulomas analyzed, we hypothesized that generation of lymphoid structures may correlate with immune control, rather than active disease. Therefore, we characterized the presence of ectopic lymphoid structures in NHPs that were experimentally infected with aerosolized *Mtb*, in which, similar to human infection, immune control results in L-TB and the absence of immune control results in A-TB (26). In support of our hypothesis, 100% of lung sections from NHPs with L-TB had

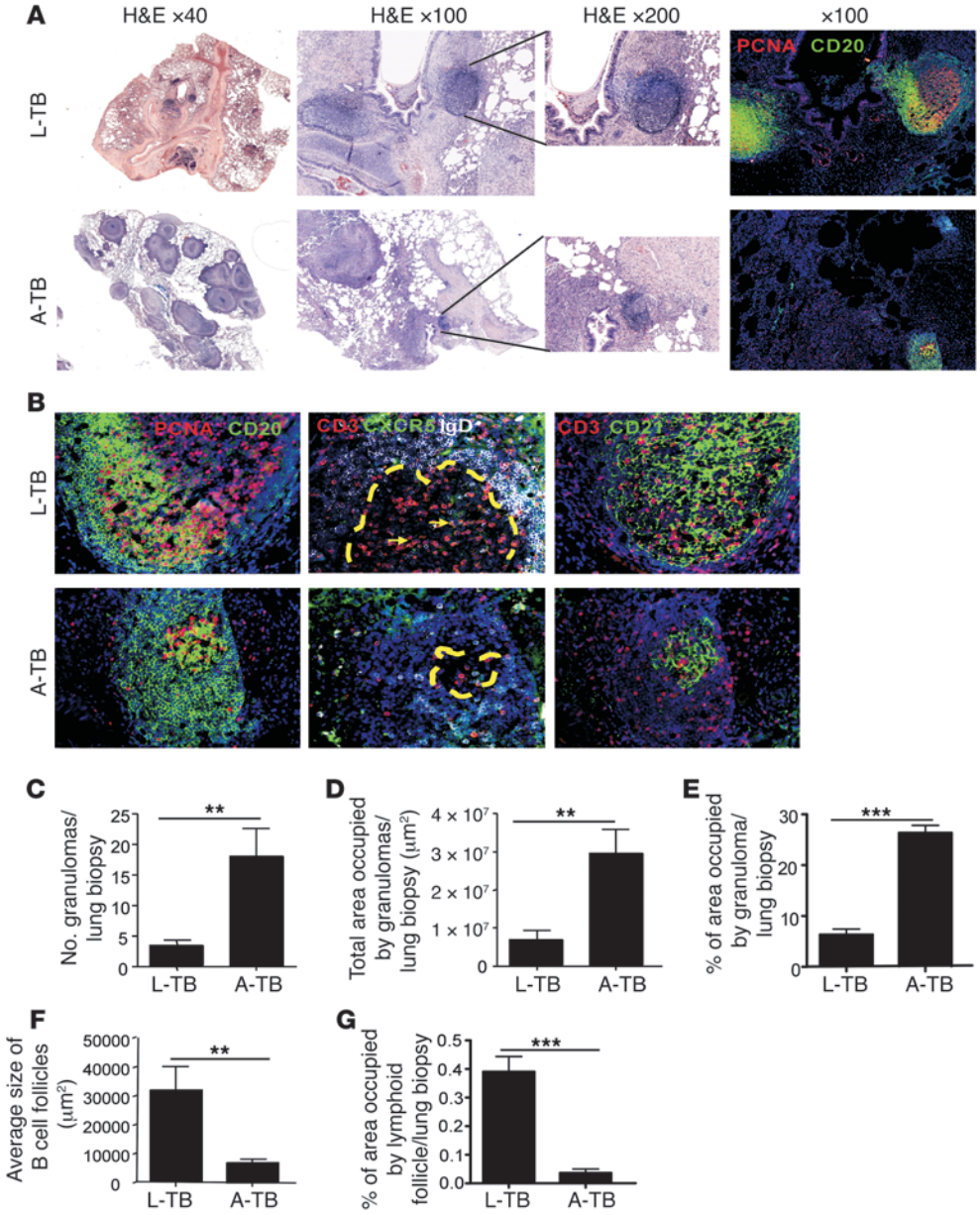

Figure 2

Ectopic lymphoid structures are associated with immune control during TB in the NHP model of *Mtb* infection. NHPs aerosol infected with *Mtb* CDC1551 exhibited either L-TB or A-TB as described in Methods. Thirteen weeks after infection or at necropsy, lung FFPE serial sections were stained with H&E (**A**) or analyzed by immunofluorescence for PCNA, CD20 (**A** and **B**), or CD3, CXCR5, IgD; CD3, CD21 (**B**). All sections were counterstained with DAPI (blue). GC, containing large, proliferating B blasts (PCNA$^+$CD20$^+$), is outlined in dashed yellow lines. Yellow arrows point to typical CD3$^+$CXCR5$^+$ T cells within lymphoid structures. The images shown are from a typical representative section. Number of granulomas (**C**), total area occupied by granulomas (**D**), percentage of granuloma area occupied per biopsy (**E**), and average size and percentage of area occupied by B cell lymphoid follicles (**F** and **G**) were determined with the morphometric tool of the Zeiss Axioplan microscope. Original magnification, ×200, unless otherwise indicated. The data points represent the mean (±SD) of values from 6–15 NHPs (**A**–**G**). $^{**}P$ = 0.005, $^{***}P$ = 0.0005.

well-organized ectopic lymphoid structures (Figure 2A and Supplemental Table 2), with distinct B cell follicles containing proliferating CD20$^+$ B cells, CXCR5$^+$ T cells, and CD21$^+$ FDC networks (Figure 2B). In contrast, in NHPs with A-TB, only 46% of lung samples contained ectopic lymphoid structures (Figure 2A and Supplemental Table 2), which were smaller, less organized, and diffuse. Furthermore, only 33% of samples from NHPs with A-TB contained proliferating CD20$^+$ B cells, CD21$^+$ FDC networks, and CXCR5$^+$ T cells (Figure 2B and Supplemental Table 2). Uncontrolled disease was also evident in NHPs with A-TB, as a large number of necrotic granulomas occupied much of the total lung area (Figure 2, C–E); despite this, lungs from NHPs with L-TB had significantly larger B cell follicles, which occupied a significantly larger area of the lung biopsy (Figure 2, F and G), contrasting with the smaller B cell follicles detected in NHPs with A-TB (Figure 2, F and G). These data demonstrate that in NHPs, generation of well-organized lymphoid structures containing CXCR5$^+$ T cells and B cell follicles is associated with immune control in L-TB, while loss of immune control during A-TB is associated with absent or loosely organized lymphoid aggregates.

Pulmonary CD4$^+$CXCR5$^+$ T cells express markers of both Th1 cells and Tfh cells. Since CXCR5$^+$ T cells were associated with immune control, we next addressed the role of CD4$^+$CXCR5$^+$ T cells in a well-established mouse model of TB in which effective host immunity results in chronic infection. Although murine TB granulomas do not demonstrate all the characteristics of human TB granulomas (27), murine granulomas also form organized lymphoid structures containing CXCR5-expressing T cells (CD3$^+$CXCR5$^+$) and B220$^+$ B cells (Figure 3A). GC B cells were identified as large, proliferating PCNA$^+$B220$^+$ blasts that bound peanut agglutinin (PNA) and contained complex FDC networks (Figure 3B). In addition, CXCL13 protein (Figure 3B) and *Cxcl13* mRNA expression was detected

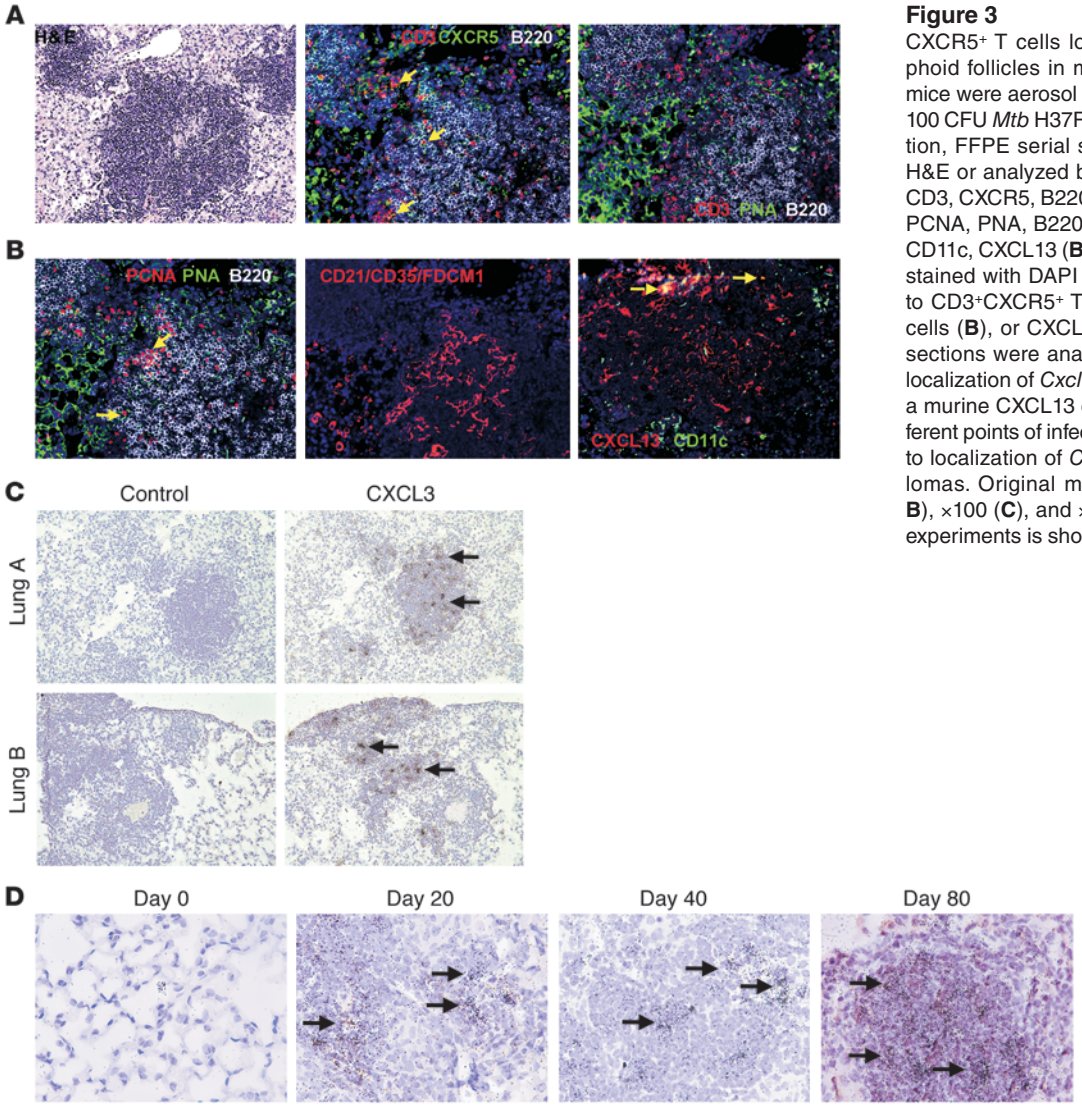

Figure 3
CXCR5$^+$ T cells localize within ectopic lymphoid follicles in murine TB granulomas. B6 mice were aerosol infected with approximately 100 CFU *Mtb* H37Rv, and on day 50 after infection, FFPE serial sections were stained with H&E or analyzed by immunofluorescence for CD3, CXCR5, B220; and CD3, PNA, B220 (**A**); PCNA, PNA, B220; CD21-CD35-FDCM1; and CD11c, CXCL13 (**B**). All sections were counterstained with DAPI (blue). Yellow arrows point to CD3$^+$CXCR5$^+$ T cells (**A**), PCNA$^+$B220$^+$ B cells (**B**), or CXCL13$^+$CD11c$^+$ cells (**B**). Lung sections were analyzed by ISH to determine localization of *Cxcl13* mRNA expression using a murine CXCL13 cRNA probe (**C**) during different points of infection (**D**). Black arrows point to localization of *Cxcl13* mRNA within granulomas. Original magnification, ×200 (**A** and **B**), ×100 (**C**), and ×600 (**D**). One of 2 or more experiments is shown.

inside lymphoid structures (Figure 3C), and expression increased over the course of infection (Figure 3D).

Given that ectopic lymphoid structures associated with TB granulomas contained CXCR5$^+$ T cells, we next tested whether these cells were functionally important. The accumulation of activated, IFN-γ–producing CD4$^+$ T cells normally occurs in the murine lung between days 15 and 21 following low-dose *Mtb* infection (22, 28). We found that activated CD4$^+$CXCR5$^+$ T cells also accumulated in the lungs between days 15 and 21 (Figure 4A). Notably, CXCR5$^+$ T cells were found at a higher frequency and number in the activated CD44^{hi}CD4$^+$ T cell subset when compared with the unactivated naive CD4$^+$CD44^{lo} T cell subset (Figure 4B). In contrast, although a population of lung B cells also expressed CXCR5, this population did not increase in frequency following *Mtb* infection (data not shown). Furthermore, B cell–deficient mice are not susceptible to low-dose *Mtb* infection (29, 30), suggesting that CD4$^+$CXCR5$^+$ T cells, rather than CXCR5$^+$ B cells, play a dominant role in protective immunity in the low-dose model of *Mtb* infection. In addition, lung activated CD4$^+$CXCR5$^+$ T cells expressed significantly higher levels of the Tfh-like cell markers ICOS and PD-1 when compared with activated CD4$^+$CXCR5$^-$ T cells and unactivated naive CD4$^+$ T cells (Figure 4C). Importantly, we found that the ICOS$^+$PD-1$^+$ CD4$^+$ T cell population increased during infection (Supplemental Figure 1A) and was enriched for expression of CXCR5 and CD44 (Supplemental Figure 1B). As expected (31), activated CD4$^+$CXCR5$^-$ T cells also expressed ICOS and PD-1, albeit at reduced levels (Figure 4C). Interestingly, activated CD4$^+$CXCR5$^+$ T cells also expressed the highest levels of the proinflammatory cytokines IFN-γ, TNF-α, and IL-2 (Figure 4D), individually or in combination, and cytokine production by CXCR5$^+$ T cells was *Mtb* specific (Supplemental Figure 1, C and D). However, only a small population of CD4$^+$CXCR5$^+$ T cells produced IL-17 and IL-21 (Supplemental Figure 1C). Despite increased proinflammatory cytokine production in activated CD4$^+$CXCR5$^+$ T cells, there were no differences in overall percentage (Supplemental Figure 1C) or numbers of cytokine-producing cells between activated CD4$^+$CXCR5$^+$ and CD4$^+$CXCR5$^-$ T cells (data not shown). In addition, the CD4$^+$CXCR5$^+$ population expressed higher levels of Bcl6, while expressing levels of Tbet similar to those in CD4$^+$ CXCR5$^-$ T cell populations (Figure 4E). These data together suggest that

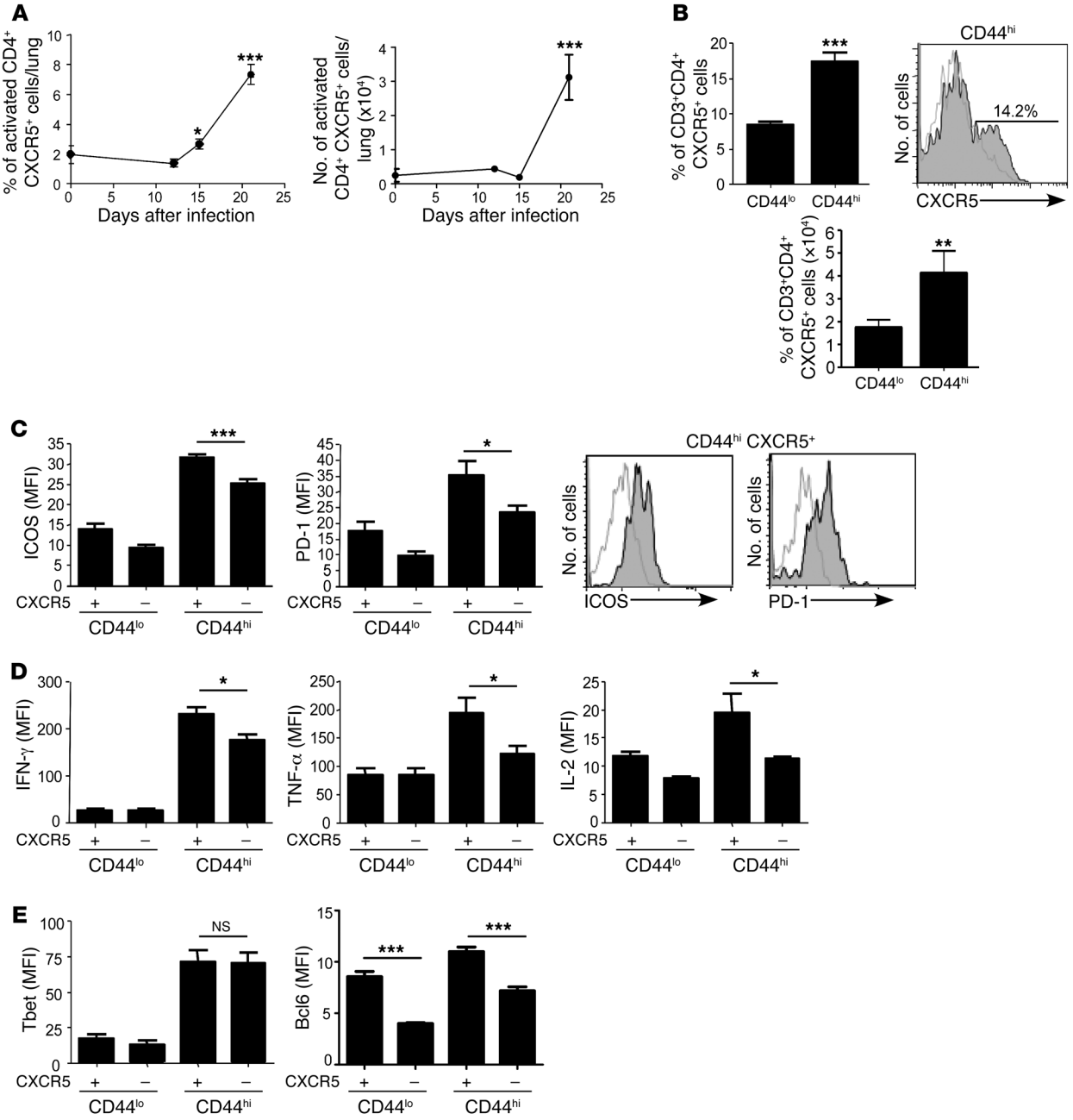

Figure 4

Activated CD4+CXCR5+ T cells accumulate in the lung during *Mtb* infection and express both Tfh-like and Th1-like cell markers. B6 mice were infected as in Figure 3. (**A**) The frequency and number of activated CD4+CXCR5+ T cells were determined by flow cytometry at different time points after infection. (**B**) Frequency and number of activated ($CD44^{hi}$) and unactivated ($CD44^{lo}$) CD4+CXCR5+ T cells were determined in *Mtb*-infected lungs on day 25 after infection by flow cytometry. A typical histogram showing CXCR5-specific staining (filled) within activated CD4+ T cells and relevant isotype control antibody (open) is shown (**B**). Expression of ICOS and PD-1 (**C**), IFN-γ, TNF-α, and IL-2 (**D**), and Tbet and Bcl6 (**E**) on activated ($CD44^{hi}$) and unactivated ($CD44^{lo}$) CD4+CXCR5+ and CD4+CXCR5– T cells was calculated by determining the mean fluorescence intensity using flow cytometry. A typical histogram showing expression of PD-1 and ICOS (filled) and relevant isotype control antibody (open) on activated CD4+CXCR5+ cells is shown (**C**). The data points represent the mean (±SD) of values from 4–6 mice (**A**–**E**). **P* = 0.05, ***P* = 0.005, ****P* = 0.0005. One experiment representative of 2.

activated CD4+ T cells express markers characteristic of Tfh-like cells such as ICOS, PD-1, and Bcl6, but also exhibit markers of Th1-like cells, such as production of proinflammatory cytokines and expression of Tbet.

We then determined whether activated CD4+CXCR5+ T cells expressed other chemokine receptors, such as CXCR3, which are associated with *Mtb*-induced lung inflammatory T cell accumulation (32). We detected expression of CXCR3 on a population of

activated CD4+ T cells (Supplemental Figure 2A) and found that a subset of CXCR3+CD4+ T cells also coexpressed CXCR5 (Supplemental Figure 2B). Surprisingly, we found that the CD4+CXCR5+ T cell subset expressed the highest frequency and expression levels of IFN-γ (Supplemental Figure 2C) and other proinflammatory cytokines (data not shown), when compared with activated CD4+CXCR3+ or CD4+CXCR3+ CXCR5+ T cell populations within *Mtb*-infected lungs (Supplemental Figure 2C). Furthermore, in contrast to the localized expression of *Cxcl13* mRNA observed within lymphoid follicles (Figure 3D), we found that mRNA for *Cxcl9*, a CXCR3 ligand, was localized both within the inflammatory lesions and near blood vessels in the *Mtb*-infected murine lung (Supplemental Figure 2D) and latently infected NHPs (Supplemental Figure 2E). These data together suggest that *Mtb*-induced inflammatory chemokines such as CXCL9 are expressed near blood vessels and likely recruit activated CD4+ T cells to the lung, but that CXCR5-CXCL13 interactions may be specifically required to localize potent cytokine-producing CD4+ T cells within the lung parenchyma to organize lymphoid follicles and maximize mycobacterial control within granulomas.

CXCR5 expression is required for strategic CD3+ T cell positioning and lymphoid follicle formation during murine TB. To determine whether there was a protective role for CXCR5 in immunity against TB, CXCR5-deficient (*Cxcr5*$^{-/-}$), mice were infected with *Mtb* and found to harbor greater lung bacterial burdens during early and chronic stages of infection, when compared with C57BL/6 (B6) mice (Figure 5A). In addition, CXCL13 neutralization also resulted in increased bacterial burden (Figure 5A), and both *Cxcr5*$^{-/-}$ and *Cxcl13*$^{-/-}$ mice demonstrated decreased survival in response to high-dose *Mtb* infection (Figure 5B). Using the low-dose *Mtb* infection model, we found that the accumulation of total B cells (Supplemental Figure 3A) was similar in B6 and *Cxcr5*$^{-/-}$ *Mtb*-infected lungs, while *Cxcr5*$^{-/-}$ *Mtb*-infected lungs showed impaired accumulation of lung GC B cells (Supplemental Figure 3B). Furthermore, no differences in levels of early secreted antigenic protein 6–specific (ESAT-6–specific) IgG1, IgG2a, and IgG2b antibodies were found in B6 and *Cxcr5*$^{-/-}$ *Mtb*-infected mice (data not shown). Therefore, we next assessed T cell responses and found that despite lack of mediastinal lymph nodes and defective splenic architecture in *Cxcr5*$^{-/-}$ mice (33), comparable percentages of IFN-γ–producing CD4+ cells (Supplemental Figure 3, C and D) and numbers of *Mtb*–ESAT-6–specific, IFN-γ–producing CD4+ cells (Supplemental Figure 3, E and F) were present in the lungs and spleen of *Cxcr5*$^{-/-}$ and B6 *Mtb*-infected mice. In addition, neither differences in frequency of total CD4+ T cells producing TNF-α and IL-2 (data not shown) nor differences in expression levels of IFN-γ, TNF-α, and IL-2 within CD4+ T cells were observed in B6 and *Cxcr5*$^{-/-}$ *Mtb*-infected lungs (data not shown). The percentage of CD4+ T cells expressing the Tfh-like cell markers ICOS and PD-1 (Supplemental Figure 3G) and the ability of activated ICOS+ PD-1+ Th cells to produce IFN-γ (Supplemental Figure 3H), TNF-α, and IL-2 (data not shown) were also similar in B6 and *Cxcr5*$^{-/-}$ *Mtb*-infected lungs. To then address whether *Cxcr5*$^{-/-}$ T cells had the potential to differentiate into cytokine-producing Th cell subsets, we immunized B6 and *Cxcr5*$^{-/-}$ mice with ESAT-6 peptide in adjuvant and expanded splenic CD4+ T cells in vitro in the presence of Th1 or Tfh cell differentiation conditions. Similar to B6 CD4+ T cells, *Cxcr5*$^{-/-}$ CD4+ T cells produced IFN-γ in response to Th1 polarizing conditions (Supplemental Figure 4A) and produced IL-21 in response to Tfh cell differentiation conditions (Supplemental Figure 4B). These data suggest that in the absence of CXCR5, B cells and cytokine-producing antigen-specific T cells accumulate efficiently in the *Mtb*-infected lung.

We therefore next addressed whether the increased susceptibility in the *Cxcr5*$^{-/-}$ mice was due to defects in localization of T cells within lung inflammatory lesions. In support of a role for CXCR5 in correct T cell localization inside granulomas, CD3+ T cells were dispersed throughout the organized lung granulomas in the B6 *Mtb*-infected mice (Figure 5C). However, CD3+ T cells were found as distinct perivascular cuffs in *Cxcr5*$^{-/-}$ *Mtb*-infected lungs and B6 mice that received CXCL13 neutralizing antibody (Figure 5, D and E), resulting in disrupted granuloma formation (Figure 5, C and D) and defective lymphoid structure generation (Supplemental Figure 4, C and D). These data together suggest that the increased susceptibility to *Mtb* infection seen in the *Cxcr5*$^{-/-}$ mice is due not to impaired priming, generation, or accumulation of cytokine-producing Tfh-like cells in the *Mtb*-infected lungs, but rather to the inability of cytokine-producing CD4+ T cells to localize correctly within the *Mtb*-infected lung, likely to activate local macrophages to control *Mtb*. We next addressed whether B cell lymphoid follicle formation within TB granulomas was a consequence of correct T cell localization and therefore a correlate of protection, but by itself not necessary for mediating the immune protection in *Mtb*-infected mice. We found that *Mtb*-infected B cell–deficient (μ*MT*$^{-/-}$) mice, despite exhibiting disrupted granuloma formation and poorly formed lymphoid follicles in the lungs (Supplemental Figure 5A), still controlled infection (Supplemental Figure 5B), as previously described (29, 30). In addition, B cell–deficient *Mtb*-infected mice generated and recruited similar numbers of ICOS+PD-1+CXCR5+ T cells (data not shown) and accumulated similar numbers of antigen-specific IFN-γ–producing cells to the lung (Supplemental Figure 5C). Furthermore, immune control in B cell–deficient mice coincided with well-dispersed T cells localized in the inflammatory lesions in the lungs (Supplemental Figure 5A) and resultant macrophage activation (Supplemental Figure 5A and Figure 5D). These data together suggest that an outcome of proper T cell localization within the lung parenchyma is the formation of lymphoid follicles; therefore, lymphoid follicle formation is a correlate of effective T cell localization and a correlate of protection in *Mtb* infection, but it is T cell localization near *Mtb*-infected macrophages that results in protection.

In support of a role for CXCR5/CXCL13 in T cell localization within the lung for optimal macrophage activation, we found that CD4+ T cells isolated from B6 *Mtb*-infected lungs migrated in response to CXCL13 in vitro, produced IFN-γ and expressed the Tfh-like cell markers ICOS and Bcl6 (Supplemental Figure 6, A and B). Importantly, we found that despite similar numbers of lung macrophages and DCs in B6 and *Cxcr5*$^{-/-}$ *Mtb*-infected lungs (Supplemental Figure 4, E and F), *Cxcr5*$^{-/-}$ *Mtb*-infected lungs had reduced induction of mRNA for the anti-mycobacterial molecule inducible nitric oxide synthase (*iNOS*) (Figure 5F), and fewer iNOS+ macrophage-like cells were detected within the disorganized granulomas of *Cxcr5*$^{-/-}$ and CXCL13-deficient (*Cxcl13*$^{-/-}$) *Mtb*-infected lungs (Figure 5G). Furthermore, CD11c+ DCs and macrophages sorted from *Cxcr5*$^{-/-}$ and *Cxcl13*$^{-/-}$ *Mtb*-infected lungs displayed lower *iNOS* mRNA expression when compared with cells isolated from B6 *Mtb*-infected lungs (Figure 5H). These data together suggest that expression of CXCR5 is critical for strategic positioning of effector T cells within the lung for optimal macrophage activation, subsequent organization of lymphoid follicles, and *Mtb* control.

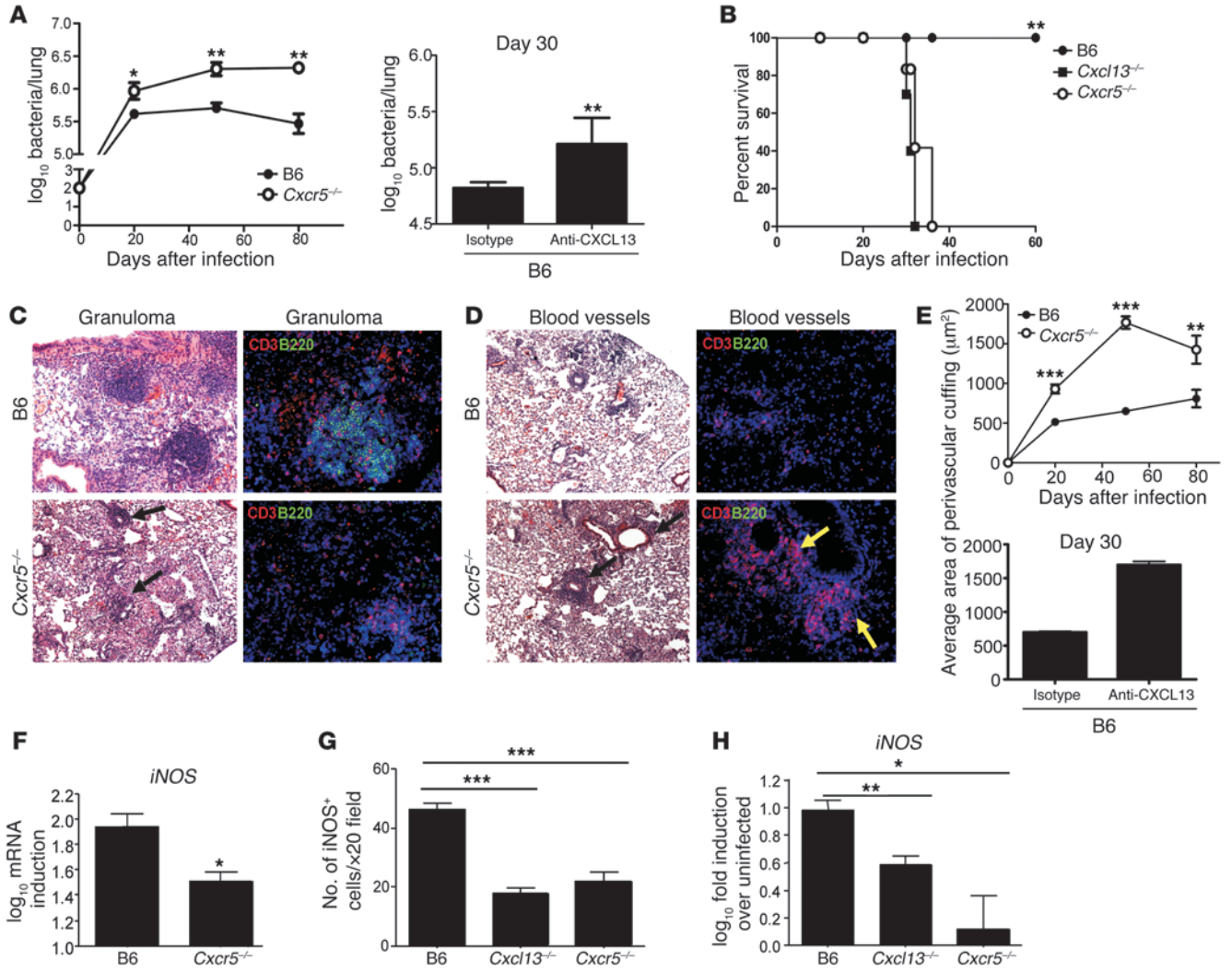

Figure 5

CXCR5 expression is required for protective immunity against *Mtb* infection. (**A**) B6 and *Cxcr5*$^{-/-}$ mice were infected as in Figure 4 or B6 *Mtb*-infected mice received CXCL13 neutralizing antibodies, and lung bacterial burden was determined. (**B**) Survival of B6, *Cxcl13*$^{-/-}$, and *Cxcr5*$^{-/-}$ mice with a high dose (1,000 CFU) of aerosolized *Mtb* infection was determined. On day 50 after infection, FFPE lung sections were H&E stained or analyzed by immunofluorescence for CD3, B220 (**C** and **D**). Representative pictures of granulomas (**C**) and perivascular T cell cuffing (**D**) are shown. Black and yellow arrows indicate T cell perivascular cuffing (**C** and **D**). (**E**) Average area of perivascular cuffs was quantified using the morphometric tool of the Zeiss Axioplan microscope. Error bars are not visible in the day 30 B6 isotype group (**E**). Original magnification, ×100 (H&E images); ×200 (fluorescent images). (**F**) $\log_{10}$ fold induction of *iNOS* mRNA in B6 and *Cxcr5*$^{-/-}$ *Mtb*-infected lungs relative to levels in uninfected lungs was determined by RT-PCR on day 21 after infection. FFPE lung sections from day 21 *Mtb*-infected B6, *Cxcr5*$^{-/-}$, and *Cxcl13*$^{-/-}$ mice were analyzed by immunofluorescence for the number of iNOS$^+$ cells per granuloma (**G**). On day 21 after infection, lung CD11c$^+$ cells were isolated from uninfected or *Mtb*-infected B6, *Cxcr5*$^{-/-}$, and *Cxcl13*$^{-/-}$ mice. (**H**) *iNOS* mRNA expression in CD11c$^+$ cells isolated from infected mice over levels detected in uninfected controls was determined by RT-PCR. The data points represent the mean (±SD) of values from 4–6 mice. (**A**–**H**). **P* = 0.05, ***P* = 0.005, ****P* = 0.0005. One experiment representative of 2 is shown.

Adoptive transfer of CD4$^+$ T cells capable of expressing CXCR5 rescues lymphoid structure formation, macrophage activation, and protection in Cxcr5$^{-/-}$ mice. Our data suggest that localization of CD4$^+$CXCR5$^+$ T cells within lymphoid structures is critical for generation of lymphoid structure formation, macrophage activation, and mycobacterial immune control. Therefore, we determined whether adoptive transfer of purified naive ESAT-6–specific Tg T cells (34), capable of expressing CXCR5, into *Cxcr5*$^{-/-}$ mice would rescue both T cell localization within the lung and macrophage activation as well as reversing susceptibility to TB. *Cxcr5*$^{-/-}$ mice that did not receive ESAT-6 Tg Th0 cells had higher bacterial burden (Figure 6A), defective lymphoid follicle generation, and reduced numbers of activated macrophages and contained numerous lymphocytic perivascular cuffs (Figure 6C). In contrast, B6 *Mtb*-infected mice formed ectopic lymphoid structures characterized by lymphocytic infiltrates (Figure 6, B and C), B cell follicles, and granulomas with considerable numbers of iNOS-expressing macrophages (Figure 6C). Importantly, adoptive transfer of ESAT-6 Tg Th0 cells into *Cxcr5*$^{-/-}$ mice decreased lung bacterial burden (Figure 6A) and restored lung lymphocytic infiltrates, T cell localization and gener-

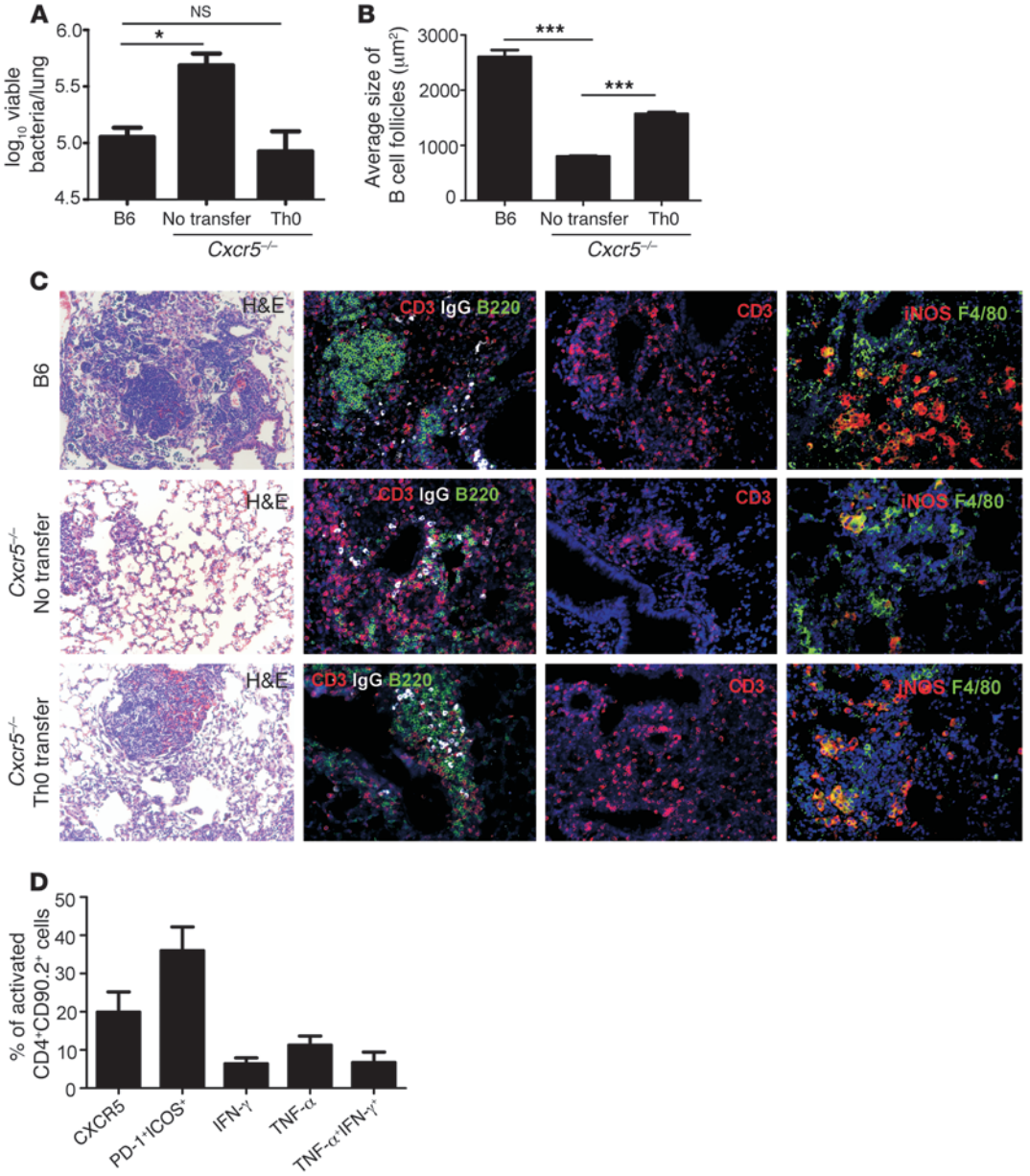

Figure 6

Adoptive transfer of ESAT-6 Tg Th0 cells rescues T cell localization and protection in *Cxcr5*$^{-/-}$ mice. 2 × 10^6 to 5 × 10^6 in vitro generated ESAT-6 Tg Th0 cells were adoptively transferred into *Cxcr5*$^{-/-}$ mice. (**A**) Twenty-four hours later, mice were infected as in Figure 3, and lung bacterial burden was determined on day 50. (**B**) The average size of B cell lymphoid follicles was quantified in B6 and *Cxcr5*$^{-/-}$ *Mtb*-infected lungs on day 50 using the morphometric tool of the Zeiss Axioplan microscope. Pulmonary granuloma and B cell lymphoid follicle formation was assessed in FFPE lung sections that were stained with H&E; CD3, IgG, B220; CD3 alone; and iNOS, F4/80 on day 50 (**B** and **C**). Original magnification, ×200 (H&E sections); ×200 (immunofluorescent sections). 2 × 10^6 to 5 × 10^6 ESAT-6 Tg CD4$^+$ Th0 cells were adoptively transferred into congenic CD90.1 B6 mice and infected as in Figure 3. (**D**) The frequency of cells expressing different molecules was determined in PMA/ionomycin-stimulated CD90.2 Tg cells isolated from infected lungs on day 21. The data points represent the mean (±SD) of values from 4–6 mice (**A**–**D**). *P = 0.05, ***P = 0.0005. NS, not significant.

ation (Figure 6C), organization of ectopic lymphoid follicles (Figure 6, B and C), and activation of lung macrophages (Figure 6C). Tracking of congenic, CD90.2$^+$ ESAT-6 Tg cells in *Mtb*-infected congenic CD90.1$^+$ mice revealed that adoptively transferred naive Tg Th0 cells had undergone activation and acquired the expression of CXCR5, ICOS, and PD-1 and the ability to produce proinflammatory cytokines (Figure 6D). Importantly, we show that the increased bacterial burden (Figure 7A) and decreased lymphoid follicle organization (Figure 7, B and C) and macrophage activation (Figure 7, C and D) in *Mtb*-infected *Cxcr5*$^{-/-}$ mice could be reversed only by adoptive transfer of CD4$^+$ T cells isolated from B6 mice, and not by transfer of CD4$^+$ T cells isolated from *Cxcr5*$^{-/-}$ mice. These data together show that adoptive transfer of uncommitted Th0 cells, capable of acquiring expression of CXCR5, restored stra-

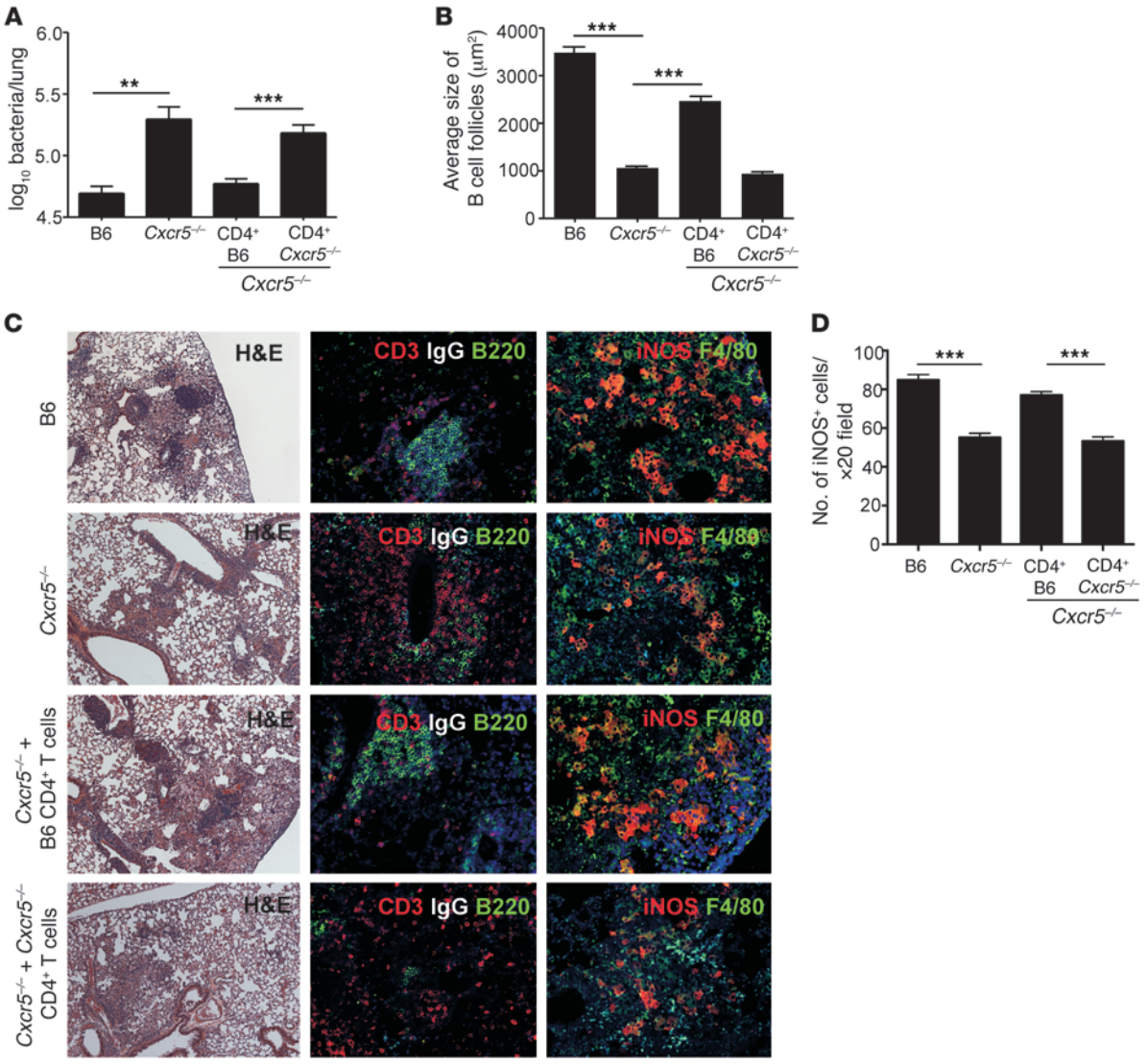

Figure 7

Adoptive transfer of B6 but not *Cxcr5*$^{-/-}$ CD4$^+$ T cells rescues T cell localization and protection in *Cxcr5*$^{-/-}$ *Mtb*-infected mice. (**A**) 2 × 10^6 CD4$^+$ B6 or *Cxcr5*$^{-/-}$ T cells were adoptively transferred into *Cxcr5*$^{-/-}$ mice. Twenty-four hours later, mice were infected as in Figure 3, and lung bacterial burden was determined on day 50. (**B**) The average size of B cell lymphoid follicles was determined in FFPE lung sections on day 50 using the morphometric tool of the Zeiss Axioplan microscope. Pulmonary granuloma and B cell lymphoid follicle formation were assessed in FFPE lung sections that were stained with H&E; CD3, IgG, B220; iNOS, F4/80 on day 50 (**B** and **C**). (**D**) iNOS$^+$ cells were quantitated using the Zeiss Axioplan microscope. Original magnification, ×50 (H&E sections); ×200 (immunofluorescent sections). The data points represent the mean (±SD) of values from 4–6 mice (**A**–**D**). $^{**}P = 0.005$, $^{***}P = 0.0005$.

tegic T cell localization within the lung and formation of lymphoid structures and reversed susceptibility to TB.

IL-21 and IL-6 are required for polarization of Tfh cells (35–37). Coincident with the early accumulation of CD4$^+$CXCR5$^+$ Tfh-like cells in *Mtb*-infected lungs, *Il6*, *Il21*, *Icos*, and *PD-1* mRNA induction occurred in *Mtb* lungs infected on day 21 (ref. 28 and Supplemental Table 3). Therefore, we tested whether absence of IL-6 and IL-21 impacts protective immunity to TB and found that B cell follicle formation was reduced, but not absent, in *Il21*$^{-/-}$ and *Il6*$^{-/-}$ *Mtb*-infected lungs (Supplemental Figure 7, A, B, D, and E) and did not impact lung bacterial control during *Mtb* infection (Supplemental Figure 7, C and F). These data suggest that although IL-6 and IL-21 are required for optimal generation of lymphoid structures, either IL-6 or IL-21 alone is sufficient for mediating protective immunity against TB.

CXCL13 expression in non-hematopoietic cells is crucial for mediating early protective immunity against TB. Our data suggest that CD4$^+$CXCR5$^+$ T cells producing proinflammatory cytokines that accumulate in the lung respond to a pulmonary CXCL13 gradient. Accordingly, CXCL13 is produced by DCs (38, 39), FDCs (40–42), and stromal cells (43). Following *Mtb* infection, we detected increased expression of CXCL13 protein in lung homogenates (uninfected: 42 ± 10.03 pg/ml, *Mtb*-infected: 452.96 ± 82.3, $P = 0.001$), and CXCL13 protein was found to colocalize with lung

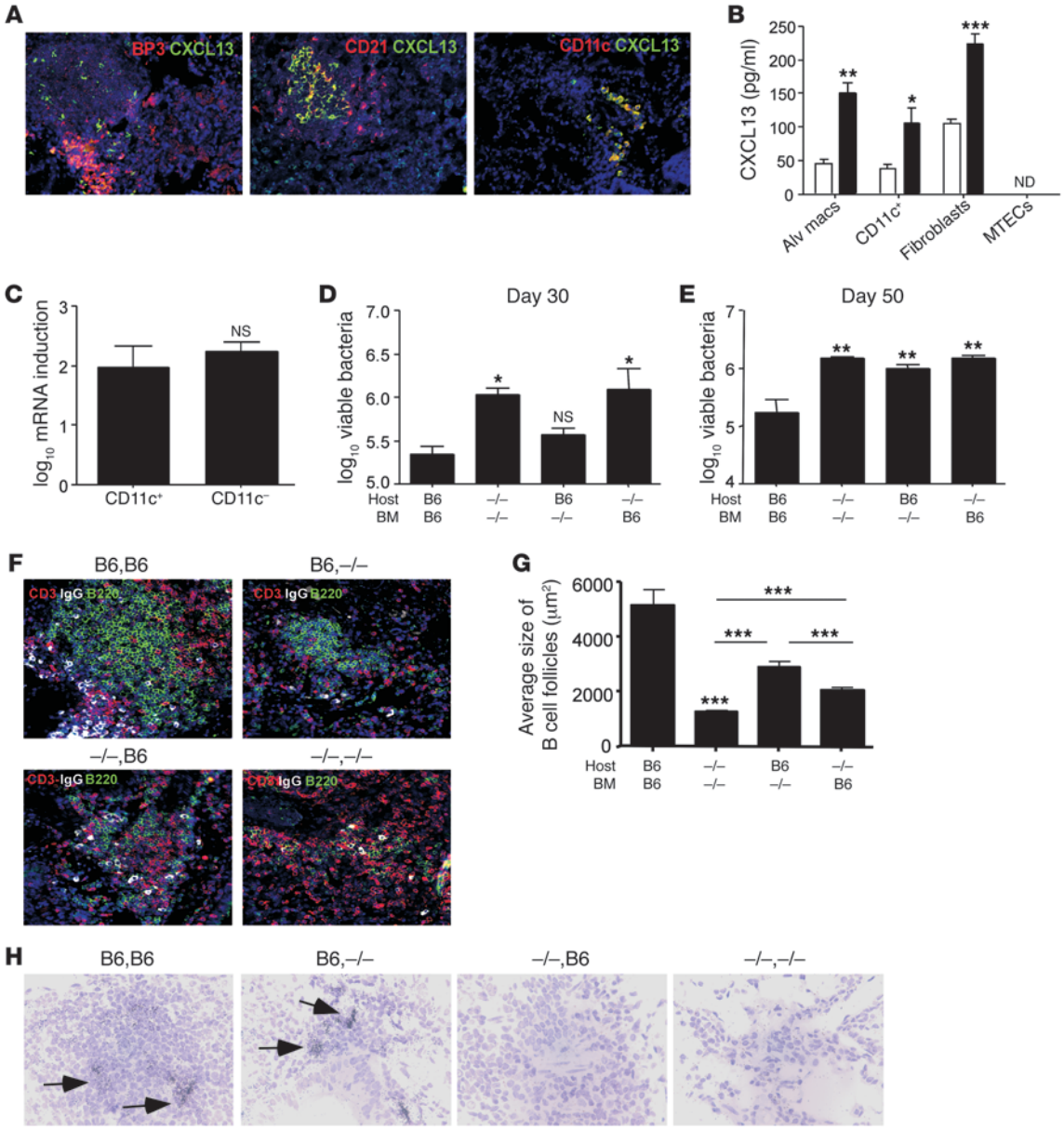

Figure 8

CXCL13 is produced by hematopoietic and non-hematopoietic cells and required for *Mtb* control. (**A**) FFPE lung sections from B6 *Mtb*-infected mice were assessed for CXCL13-producing populations by immunofluorescence. (**B**) Alveolar macrophages (Alv macs), lung CD11c$^+$ cells, lung fibroblasts, and MTECs were left untreated or treated with irradiated *Mtb* (100 μg/ml) for 24 hours and supernatants assayed for CXCL13 protein. ND, not detectable. (**C**) CD11c$^+$ and CD11c$^-$ cells were sorted from B6 *Mtb*-infected lungs (day 50 after infection), and $\log_{10}$ fold induction of *Cxcl13* mRNA was determined by RT-PCR. Hematopoietic *Cxcl13*$^{-/-}$ BMC mice (B6 host/–/– BM), non-hematopoietic *Cxcl13*$^{-/-}$ BMC mice (–/– host/B6 BM), complete *Cxcl13*$^{-/-}$ BMC mice (–/– host/–/– BM), and complete B6 BMC mice (B6 host/B6 BM) were infected with *Mtb*, and lung bacterial burden was determined on days 30 (**D**) and 50 (**E**). (**F**) Pulmonary B cell lymphoid follicles were detected in FFPE lung sections (day 50) by immunofluorescence staining for CD3, IgG, and B220; DAPI (blue) was used to detect nuclei. (**G**) Average size of the B cell lymphoid follicles was determined using the morphometric tool of the Zeiss Axioplan microscope. (**H**) Day 30 FFPE lung sections were assayed for *Cxcl13* mRNA localization by ISH. Black arrows indicate CXCL13 localization within granulomas. Original magnification, ×600 (ISH); ×200 (immunofluorescence). The data points represent the mean (±SD) of values from 3–4 samples (**A** and **B**) or from 4–6 mice (**C**–**H**). *P = 0.05, **P = 0.005, ***P = 0.0005. One experiment representative of 2 is shown.

BP3$^+$ stromal cells, CD21-CD35$^+$ FDCs, and CD11c$^+$ DCs (Figure 8A). Furthermore, when lung alveolar macrophages, CD11c$^+$ cells, mouse tracheal epithelial cells (MTECs) and fibroblasts were exposed to *Mtb* in vitro, CXCL13 protein was detected in supernatants from myeloid cells and fibroblasts, but not epithelial cell supernatants, suggesting that both hematopoietic and non-hematopoietic cells produce CXCL13 during *Mtb* infection (Figure 8B). Also, both CD11c$^+$ and CD11c$^-$ cells isolated from *Mtb*-infected B6

lungs expressed *Cxcl13* mRNA (Figure 8C). To delineate the protective contributions of CXCL13 production by hematopoietic and non-hematopoietic cells, we infected hematopoietic *Cxcl13*$^{-/-}$ bone marrow chimeric (BMC) mice (B6 host/–/– BM) or non-hematopoietic *Cxcl13*$^{-/-}$ BMC mice (–/– host/B6 BM) with *Mtb*. As expected (19), complete *Cxcl13*$^{-/-}$ BMC mice (–/–host/–/– BM) were more susceptible to *Mtb* infection than complete B6 BMC mice (B6 host/B6 BM) (Figure 8D). Interestingly, non-hematopoietic, but not hematopoietic *Cxcl13*$^{-/-}$ BMC mice had increased lung bacterial burden at early time points (Figure 8D), while at later time points, both hematopoietic and non-hematopoietic *Cxcl13*$^{-/-}$ BMC mice had increased lung bacterial burden (Figure 8E), decreased T cell localization within the lung, and reduced lymphoid structure formation when compared with B6 *Mtb*-infected lungs (Figure 8, F and G). Furthermore, hematopoietic *Cxcl13*$^{-/-}$ BMC mice, which were protected during early infection, had more distinct T cell localization within the lung, highly organized B cell lymphoid follicle structures (Figure 8, F and G), and increased *Cxcl13* mRNA expression within lymphoid structures (Figure 8H). These data show that both hematopoietic and non-hematopoietic sources of CXCL13 are required for lymphoid structure formation and protective immunity against *Mtb* infection, but that non-hematopoietic sources of CXCL13 are required for early protective immunity during TB.

Discussion

Granulomas are found in both latent and active forms of TB (27). However, the immunological differences between a "functional" granuloma that limits infection during L-TB and one that is incapable of controlling infection during A-TB is not clear (27). Consistent with previous studies, we show that lymphocytic aggregates associated with TB granulomas in mice (18), NHPs (4), and humans (3, 7) exhibit markers associated with ectopic lymphoid tissues, including proliferating GC B cells, CXCR5$^+$ T cells, and FDC networks, and colocalize with macrophages. Importantly, our experiments in NHPs show for the first time that the formation of organized ectopic lymphoid tissues containing CXCR5$^+$ T cells within granulomas is associated with better protective outcomes during L-TB, while disorganized lymphoid aggregates coinciding with poor CXCR5$^+$ T cell localization are associated with poor protective outcomes, as in A-TB. Furthermore, our mechanistic studies with mice show that CD4$^+$CXCR5$^+$ T cells exhibit characteristics of Tfh-like cells, while simultaneously expressing markers of Th1 cells. Our data suggest that activated cytokine-producing CD4$^+$ T cells express CXCR5 as a means to instruct correct localization of Tfh-like cells within the lung parenchyma to activate infected macrophages for optimal control of *Mtb*. Our data also demonstrate that a consequence of proper T cell localization within the lung is formation of ectopic lymphoid structures that serve as a useful correlate of protection, but that B cell follicle formation by itself is not protective in the mouse model of TB. Thus, our results have far-reaching implications for the future design of vaccines and therapies to prevent and treat TB.

Our studies using *Cxcr5*$^{-/-}$ mice demonstrate that expression of CXCR5 is required for T cell localization within the lung and macrophage activation for *Mtb* control. *Cxcr5*$^{-/-}$ mice lack mediastinal lymph nodes and exhibit defective splenic architecture (33) but, following *Mtb* infection, generate comparable numbers of antigen-specific cytokine-producing CD4$^+$ T cells in the lymphoid organs and accumulate in the lung. These data are consistent with previous work (10) showing that immunization of host mice with antigen in adjuvant resulted in similar expression of ICOS, CD40L, IFN-γ, and IL-4 in adoptively transferred CXCR5-deficient T cells compared with wild-type T cells. Similarly, CXCR5 expression was not required for the expression of Tfh-like markers ICOS and PD-1, production of proinflammatory cytokines, or expression of the Th1 markers Tbet and CXCR3 (data not shown) in CD4$^+$ T cells in our model. This is also consistent with the findings in mice lacking SLOs, which are still able to control *Mtb* infection and induce effective adaptive T cell responses that presumably prime in the lung (20). That similar numbers of lung myeloid cells accumulate in *Cxcr5*$^{-/-}$ *Mtb*-infected lungs but exhibit reduced activation suggests that absence of CXCR5-mediated T cell localization within the lung results in impaired ability to activate myeloid cells to control intracellular *Mtb* replication. Importantly, we show that adoptive transfer of ESAT-6 Tg T cells or wild-type CD4$^+$ T cells that can express CXCR5 into *Mtb*-infected *Cxcr5*$^{-/-}$ mice allows T cells to localize within the lung, activate macrophages, reverse generation of ectopic lymphoid structures, and confer protection against *Mtb* infection. These data demonstrate that expression of CXCR5 on T cells is critical for correct T cell localization within the lung parenchyma, likely maximizing macrophage T cell interaction and promoting optimal *Mtb* control. Although these studies suggest a direct role for CXCR5 on T cells in CXCL13 responsiveness and T cell localization, it is also possible that CXCR5 expression regulates the expression of additional adhesion molecules or other homing receptors on T cells to impact T cell localization, and this should be further explored. In this context, the ligand for CXCR5, CXCL13, is induced in ectopic lymphoid tissues in response to infection and inflammation (6, 21, 44). During *Mtb* infection, stromal cells, FDCs, and CD11c$^+$ DCs all produce CXCL13. We show here that CXCL13 expression by non-hematopoietic cells is critical for early production of CXCL13 and immunity, but that both non-hematopoietic and hematopoietic sources of CXCL13 are required for long-term control of *Mtb*. Since both stromal cells and FDCs (derived from stromal cells or fibroblasts; refs. 45–47) express CXCL13 in *Mtb* lesions, non-hematopoietic cells likely first respond to infection or infection-induced cytokines, produce CXCL13, and recruit T cells within the lung parenchyma to activate macrophages and facilitate lymphoid structure formation. These data show for the first time that differential cellular sources of CXCL13 in ectopic lymphoid tissues can impact progression of disease and protective outcomes in chronic infections, suggesting that targeting CXCR5/CXCL13 expression may be a powerful tool to improve vaccine strategies and therapy against TB.

In vitro generated Tfh cells are thought to express different cytokines compared with either Th1 or Th2 cells (36), but in vivo generated Tfh-like cells can express Th1 (48, 49), Th2 (48–51), or Th17 cytokines (35) in SLOs. Immunization with a protein antigen in adjuvant (48) or infection with *Leishmania major* (49) and *Toxoplasma gondii* (52) induces IFN-γ production in Tfh-like cells, and B cells isolated from the Tfh-B cell conjugates showed evidence of IFN-γ–induced class switch toward IgG2a (49). In contrast, IL-4–producing Tfh-like cells are found following infection with *Schistosoma mansoni* (51) or *Heligmosomoides polygyrus* (50) — both models that induce classic Th2 responses. However, recent studies show that Tfh cells are plastic (53) and that Th1 cells and Tfh-like cells share a transitional stage, during which expression of both Th1 and Tfh cell markers occurs (52). Our data support this model, as during *Mtb* infection, CD4$^+$ T cells co-exhibit markers expressed by both Tfh and Th1 cells and utilize the characteristics of both

these T helper subsets to mediate protective immunity against *Mtb* infection. For example, production of proinflammatory cytokines by T cells is crucial for protective immunity against TB in both humans and mice (22), and studies indicate that expression of multiple proinflammatory cytokines by CD4+ T cells may provide maximal control of *Mtb* infection (54). This is consistent with our study, where we found that activated CD4+CXCR5+ cells that accumulate in the *Mtb*-infected lung are the most potent producers of multiple proinflammatory cytokines. In addition, the presence of CXCR3 and/or CXCR5 on activated CD4+ T cells suggests that T cell responsiveness to multiple chemokines may benefit the host. It is possible that activated CD4+ T cells express CXCR3 and accumulate in the inflamed lung in response to CXCR3 ligands, then downregulate CXCR3 and upregulate expression of both CXCR5 and proinflammatory cytokines to respond to infection-induced CXCL13 for localization near infected macrophages for *Mtb* control. Consistent with this hypothesis, *Cxcr3*$^{-/-}$ mice are not more susceptible to low-dose *Mtb* infection, despite having defects in early neutrophil recruitment and granuloma formation (32). In addition, mice lacking other chemokine receptors, such as CCR5 (55), CCR2 (56), and CCR7 (18), are not more susceptible to low-dose *Mtb* infection, while absence of CXCR5 or CXCL13 (19) results in increased susceptibility to TB. These data together suggest that while some chemokine receptor ligands are redundant, the CXCR5/CXCL13 axis plays a unique and non-redundant function in orienting activated proinflammatory cytokine-producing CD4+ T cells near activated macrophages to mediate protective immunity to TB.

The role for B cells and humoral immunity in protection against *Mtb* infection is an emerging area of research, as some components of the humoral immune response such as Fc receptors (57) have been shown to impact immune responses to TB. Importantly, B cell follicles containing proliferating B cells have been found to colocalize with T cells within human TB granulomas (3, 7), A-TB in NHPs (4), and *Mtb*-infected mouse granulomas (18, 19). Surprisingly, B cell–deficient mice are not more susceptible in a physiologically relevant low-dose aerosol *Mtb* infection model in published studies (29, 30), as well as in this study. In addition, our data show that although *Mtb*-infected B cell–deficient mice do not form obvious ectopic lymphoid structures, they accumulate CXCR5+ CD4+ T cells capable of producing proinflammatory cytokines in the lung and localize within the lung parenchyma for macrophage activation and *Mtb* control. This is further supported by our adoptive transfer studies, where WT CD4+ T cells, but not *Cxcr5*$^{-/-}$ CD4+ T cells, upon transfer into *Cxcr5*$^{-/-}$ *Mtb*-infected mice can rescue T cell localization within the lung, macrophage activation, and *Mtb* control and facilitate B cell follicle formation. These data together suggest that formation of B cell follicles within ectopic lymphoid structures is a consequence of correct T cell localization within the lung and can be effectively used as a correlate of protection against *Mtb* infection, but itself may not be necessary for *Mtb* control. The potential protective role of B cell follicles in immunity to *Mtb* infection in humans is a challenging but crucial question that needs to addressed in future mechanistic studies.

In summary, we show that activated CD4+CXCR5+ T cells accumulate in the *Mtb*-infected lung, express markers of both Th1-like and Tfh-like cells, respond to infection-induced CXCL13, and strategically localize within the lung parenchyma, activating macrophages and accelerating control of *Mtb* and forming ectopic lymphoid structures. These results show a novel and previously undescribed role for CD4+CXCR5+ Th cells in the orchestration of protective immunity via macrophage activation. These properties of CD4+CXCR5+ T cells could therefore be exploited to mediate more localized immunity and protection against intracellular pathogens such as *Mtb* and targeted to improve vaccine strategies against pulmonary pathogens.

Methods

Human tissue samples and patient diagnosis. Archival paraffin samples of human lung biopsies with diagnosis of TB were collected according to a protocol approved by the Ethics Committee of the Instituto Nacional de Enfermedades Respiratorias and the Ethics Committee of the American British Cowdray Medical Center, Mexico City (Supplemental Table 1). All subjects were of similar socioeconomic status and unrelated to the third generation as determined by a questionnaire. TB cases had symptoms (weight loss >10 kg, cough, fever, night sweats for >1 month, or cervical or axillary lymphadenopathy) and chest radiographic findings consistent with recent pulmonary TB, a positive sputum acid-fast smear, and culture confirmed for *Mtb*. Once the diagnostic protocol was completed, patients were discharged, and proper treatment was indicated.

Mtb infection in NHPs. Groups of NHPs (Indian rhesus macaques) were used in this study at the Tulane National Primate Research Center as previously described following the recommendations of the Institutional Animal Care and Use Committee (26). For L-TB, NHPs were infected with a low dose of *Mtb* CDC1551 (200–500 CFU) by the aerosol route (26). *Mtb* exposure was confirmed by positive tuberculin skin test and PRIMAGAM (Prionics), a quantiferon-type IFN-γ release assay specifically designed to confirm *Mtb* infection in NHPs. The NHPs did not exhibit any clinical signs of TB, as evident from normal body temperatures and weights, chest x-rays, and serum levels of acute phase proteins (26). For A-TB, NHPs were infected with a high dose of *Mtb* CDC1551 via aerosol infection (~5,000 CFU) (58). *Mtb* exposure was confirmed by positive tuberculin skin test and PRIMAGAM, and the NHPs exhibited clinical signs of TB, as evident from body temperatures, weights, and chest x-rays (58).

Mtb infection in mice. B6, *Il6*$^{-/-}$, μ*MT*$^{-/-}$, *Cxcl13*$^{-/-}$, and *Cxcr5*$^{-/-}$ mice on the B6 background were purchased from The Jackson Laboratory. *Il21*$^{-/-}$ mice were obtained from the Mutant Mouse Regional Resource Center (MMRC) and backcrossed to B6 mice for 10 generations. ESAT-6 αβ TCR Tg mice recognize IA^b/ESAT-6$_{1-20}$ and were provided by G. Winslow (Wadsworth Center, Albany, New York, USA) and D. Woodland (Trudeau Institute, Saranac Lake, New York, USA) (34). The ESAT-6 TCR Tg mice were crossed and maintained on the *Rag1*$^{-/-}$ background. All mice strains were bred and maintained at the Children's Hospital of Pittsburgh's animal facility. Experimental mice were age and sex matched and used between the ages of 6 and 8 weeks in accordance with University of Pittsburgh International Animal Care and Use Committee guidelines. *Mtb* strain H37Rv was cultured in Proskauer-Beck medium containing 0.05% Tween 80 to mid-log phase and frozen in 1-ml aliquots at –70°C. Animals were aerosol infected with ~100 (low dose) or ~1,000 (high dose) CFU bacteria using a Glas-Col airborne infection system (59). At given time points, organs were harvested and homogenized, serial dilutions of tissue homogenates plated on 7H11 plates, and CFU determined. In some experiments, mice were subcutaneously vaccinated with ESAT-6$_{1-20}$ peptide (400 mg) emulsified with the adjuvant containing MPL with TDM (Sigma-Aldrich) and DDA (ACROS Organics) as described previously (60). On day 14 after vaccination, splenic CD4+ T cells were sorted and cultured with irradiated APCs and Th-polarizing conditions as described below. For generation of Th cell subsets, CD4+ T cells were cultured with BMDCs, ESAT-6$_{1-20}$ peptide, and cytokine cocktails; for Tfh cells: Iscove's complete medium containing IL-21 (50 ng/ml), anti–IL-4 (10 μg/ml), anti–IFN-γ (10 μg/ml), and IL-2 (10 U/ml); for Th1 cells: complete DMEM containing IL-12 (10 ng/ml), anti–IL-4 (10 μg/ml),

and IL-2 (10 U/ml) (36). B6 mice were aerosol infected with ~100 CFU *Mtb* H37Rv, and beginning on day 15 after infection, mice received 200 μg CXCL13 antibody or isotype control antibody (R&D Biosystems) every other day until day 30 after infection, when organs were harvested.

Morphometric analysis and immunofluorescence. Lungs from mice and NHPs were inflated with 10% neutral buffered formalin and embedded in paraffin. Lung sections were stained with H&E (Colorado Histo-Prep) and processed routinely for light microscopy. Formalin-fixed samples from TB patients were also used. For immunofluorescence, paraffin was removed from the formalin-fixed lung sections and washed with xylene, alcohol, and PBS. Antigens were unmasked using Dako Target Retrieval Solution and were blocked with 5% (v/v) normal donkey serum and Fc block (5 μg/ml, 2.4G27). Endogenous biotin was neutralized with avidin followed by biotin (Sigma-Aldrich). Murine sections were probed with goat anti–mouse CD3ε (M-20, Santa Cruz Biotechnology Inc.), rat anti–mouse B220 (RA3-6B2, BD Biosciences — Pharmingen), iNOS (goat anti-mouse, M-19, Santa Cruz Biotechnology Inc.), F4/80 (MCA497GA, Serotec), CXCR5 (biotin, rat anti-mouse CXCR5, BD Biosciences), and IgG (FITC-donkey anti-mouse IgG, Jackson Immunoresearch Laboratories Inc.). Primary Abs were detected with secondary Ab conjugated to Alexa Fluor 568 for iNOS and CD3 (Alexa Fluor 568, donkey anti-goat, Invitrogen). Donkey anti-rat Ab conjugated to Alexa Fluor 488 was used to visualize B220 (Molecular Probes, Invitrogen). Some slides were incubated with PNA-FITC (Sigma-Aldrich) and goat anti-PCNA (C-20, Santa Cruz Biotechnology Inc.). Rabbit anti-FITC, conjugated to Alexa Fluor 488, was used to amplify PNA signal (Molecular Probes, Invitrogen). To detect FDCs, slides were incubated with biotinylated rat anti–mouse CD21-CD35 (CR2/CR1, BioLegend) and anti-FDC (FDCM-1, BD Biosciences — Pharmingen), followed by detection with SA-Alexa Fluor 488 and donkey anti-rat conjugated to Alexa Fluor 488 (Molecular Probes, Invitrogen). DCs and stromal cells were stained with PE-hamster anti–mouse CD11c (HL3, BD Biosciences — Pharmingen) and PE-mouse anti–mouse CD157 (BP3, BD Biosciences — Pharmingen). To amplify the signal, a rabbit anti-PE antibody (Rockland) was used, followed by its detection with Fab, donkey anti-rabbit–Cy3 (Jackson Immunoresearch Laboratories Inc.). CXCL13 production in infected lungs was detected with goat anti–mouse CXCL13 (R&D Systems), followed by detection with donkey anti-goat–Alexa Fluor 568. Human and NHP tissues were probed with rabbit anti-human ICOS (Abcam), FITC, mouse anti–human CXCR5 (clone 51505, R&D Systems), and goat anti–human CXCL13 (R&D Systems). CD3ε was further used to detect CD3 lymphocytes (clone M-20, Santa Cruz Biotechnology Inc.). For B cells, CD20 (mouse anti–human CD20 [L26], Abcam) and IgD (Ab-1, Lab Vision Corp.) were used with PCNA (goat anti-PCNA [C-20], Santa Cruz Biotechnology Inc.) to detect GC B cells. FDCs in human GCs were further detected with anti–human CD21 (clone 2G9, Lab Vision Corp.). SlowFade Gold antifade with DAPI (Molecular Probes, Invitrogen) was used to counterstain tissues and to detect nuclei. Images were obtained with a Zeiss Axioplan 2 microscope and were recorded with a Zeiss AxioCam digital camera. Caudal lobes from 4 mice per group underwent morphometric analysis in a blinded manner using the morphometric tool of Zeiss Axioplan microscope, which determines the area defined by the squared pixel value for each granuloma, B cell follicle, and perivascular cuff, as previously described (19).

CXCL13 ISH. Mouse CXCL13 cDNA was RT-PCR amplified with primers BFJ.mCXCL13_F1 (5′-GAACTCCACCTCCAGGCAGA-3′) and BFJ.mCXCL13_R1 (5′-CTTTTGAGATGATAGTGGCT-3′). Human CXCL13 cDNA was RT-PCR amplified with primers 5′-AGACAGAATGAAGTTCATCT-3′ and 5′-GTGGAAATATCAGCATCAGGG-3′. PCR products were ligated to the pGEM-T vector (Promega) and DNA sequenced. The pGEMT-CXCL13 plasmid was linearized by restriction digest. Gene-specific riboprobes were synthesized by in vitro transcription using a Maxiscript SP6/T7 kit (Ambion), and unincorporated nucleotides were removed using RNA Mini Quick Spin Columns (Roche). Paraffin-embedded tissue specimens were pretreated as described previously (61), following deparaffinization in xylene and rinsing in ethanol. In situ hybridization (ISH) with ^{35}S-labeled riboprobes was performed at 50°C overnight as described (62), with 0.1 M dithiothreitol included in the hybridization mix. Tissue sections were coated with NTB-2 emulsion (Kodak) and exposed at 10°C for 10 days. The sections were counterstained with hematoxylin (Vector) and mounted with Permount (Fisher). Images were visualized using an Olympus BX41 microscope and captured using a SPOT RT3 digital camera (Diagnostics Instruments Inc.).

Lung and spleen single-cell preparation. Lung tissue and the spleen were prepared as previously described (63). Briefly, single-cell suspensions were prepared from digested lung tissue or spleen by dispersing the tissue through a 70-μm nylon tissue strainer (BD Falcon). The resultant suspension was treated with Gey's solution to remove residual red blood cells, washed twice, counted, and used in assays described below.

Generation of lung cell types. For generation of lung fibroblast, lungs were perfused with 5 U/ml dispase, followed by 1% low-melting-point agarose, washed in PBS, and incubated in dispase for 30 minutes at 37°C. Single-cell suspensions were then obtained from DNase/collagenase-treated lungs and fibroblasts generated by passaging 2–4 times. Lung alveolar macrophages were obtained by bronchoalveolar lavage as previously described (64). Lung CD11c$^+$ cells were sorted from single-cell lung suspensions using a magnetically labeled CD11c-positive isolation kit (Miltenyi Biotec). MTECs were generated using an air-liquid interface culture as previously described (65). All the different cell types were stimulated with irradiated *Mtb* (100 μg/ml) for 24 hours and cell supernatants analyzed for CXCL13 protein.

Real-time PCR. RNA was extracted as previously described (64). RNA was treated with DNAse and reverse transcribed, and cDNA was then amplified with an FAM-labeled probe and PCR primers on the ABI Prism 7700 detection system. The $\log_{10}$ fold induction of mRNA in experimental samples was calculated over signals derived from uninfected/control samples. In some samples, the specific gene expression was calculated relative to GAPDH expression. The primer and probes sequences targeting genes encoding iNOS have been previously published (19).

Flow cytometry. Single-cell suspensions were stained with fluorochrome-labeled antibodies specific for CD3 (145-2C11), CD4 (RM4-5), CXCR5 (2G8), IFN-γ (XMG1.2), TNF-α (MP6-XT22), IL-21 (IL-21R-FC chimeric protein), IL-2 (JES6-5H4), Tbet (clone 04-46) CD44 (IM7), Gr-1 (RB6-8C5), CD11c (HL3), CD11b (M1/70), B220 (RA3-6B2), CD19 (ID3), Ly77 (GL7), CXCR3 (CXCR3-173), Bcl6 (7MG191E), ICOS (7E.17G9), PD-1 (J43), and PNA (Sigma-Aldrich) or relevant isotype control antibodies. For intracellular analyses of cells, cells stimulated with PMA (50 ng/ml), ionomycin (750 ng/ml; Sigma-Aldrich), or ESAT-$6_{1–20}$ peptide (5 μg/ml) and GolgiStop (BD Biosciences — Pharmingen) were surface stained, permeabilized with Cytofix-Cytoperm solution (BD Biosciences — Pharmingen), and stained for relevant cytokines. Cells were read using a BD FACSAria flow cytometer using FACSDiva software. Cells were gated based on their forward-by-side scatter characteristics, and the frequency of specific cell types was calculated using FlowJo (Tree Star Inc.). The mean fluorescence intensity was also calculated to determine expression levels of different molecules using FlowJo.

Detection of IFN-γ–producing cells by ELISpot assay. ESAT-$6_{1–20}$–specific IFN-γ–producing IA^b-restricted T cells from infected lungs or spleen were enumerated using peptide-driven ELISpot as described previously (63). Briefly, 96-well ELISpot plates were coated with monoclonal anti–mouse IFN-γ, blocked with medium containing 10% FBS. Cells from lungs and spleen were seeded at an initial concentration of 5×10^5 cells/well and subsequently diluted 2-fold. Irradiated B6 splenocytes were used as APCs at a

concentration of 1×10^6 cells/well in the presence of ESAT-$6_{1–20}$ (10 μg/ml) peptide and IL-2 (10 U/ml). After 24 hours, plates were washed and probed with biotinylated anti–mouse IFN-γ. Spots were visualized and enumerated using a CTL-Immunospot S5 MicroAnalyzer. No spots were detected in cultures lacking antigen or when using cells from uninfected mice.

Adoptive transfer of CD4⁺ T cells. Naive CD4⁺ T cells were isolated from single-cell suspensions generated from lymph nodes and spleens of ESAT-6 TCR Tg, B6, and *Cxcr5*$^{-/-}$ mice using a positive CD4⁺ T cell isolation kit (Miltenyi Biotec) as described previously (19). For adoptive transfer into host mice, 2×10^6 to 5×10^6 naive T cells were transferred intravenously, after which mice were rested for 24 hours and challenged with *Mtb* H37Rv by the aerosol route.

Generation of BMC mice. To generate chimeric mice, we gave mice a medicated Sulfa-Trim diet containing 1.2% sulfamethoxazole and 0.2% trimethoprim (TestDiet) 2 weeks prior to irradiation. Mice were sublethally irradiated with 10 Gy in 2 doses (X-Rad 320). Mice were subsequently reconstituted with 10×10^6 bone marrow cells from B6 or gene-deficient mice via i.v. injection. Mice were allowed to reconstitute for 45 days while continuing to receive a Sulfa-Trim and acidified water diet, after which they were used in experimental procedures.

Protein estimation by ELISA. Mouse DuoSet ELISA antibody pairs from R&D Systems were used to detect CXCL13, IFN-γ, and IL-21 protein levels in the supernatant according to the manufacturer's protocol. In some experiments, protein levels were measured using a mouse Luminex assay (Linco/Millipore).

Statistics. Differences between the means of experimental groups were analyzed using the 2-tailed Student's *t* test. Differences were considered significant when *P* was less than or equal to 0.05.

Study approval. For human studies, written informed consent from participants or their guardians was received under a protocol approved by the Ethics Committee of the Instituto Nacional de Enfermedades Respiratorias and the Ethics Committee of the American British Cowdray Medical Center, Mexico City. Experimental mice were used in accordance with University of Pittsburgh International Animal Care and Use Committee guidelines.

Acknowledgments

This work was supported by Children's Hospital of Pittsburgh; NIH grants AI083541 and HL105427 to S.A. Khader, RR026006, AI091457, RR020159, and Tulane Primate Center base grant RR000164 to D. Kaushal, HL69409 to T.D. Randall, and AI060422 to T.A. Reinhart, start-up funds from the Department of Medicine, University of Rochester, and AI91036 to J. Rangel-Moreno; T32 AI065380-08 grant to S.R. Slight; and a Research Advisory Committee Grants from Children's Hospital of Pittsburgh of the UPMC Health System to S.R. Slight and Y. Lin. The authors thank John Alcorn, David Askew, Nikhil Nuthalapathi for technical help, and Hillary Cleveland for mouse breeding. The authors thank Jay Kolls, Anuradha Ray, Toni Darville, Yatin Vyas, and John Alcorn for critical reading of the manuscript.

Received for publication July 11, 2012, and accepted in revised form November 1, 2012.

Address correspondence to: Shabaana A. Khader, Division of Infectious Diseases, Children's Hospital of Pittsburgh of UPMC, University of Pittsburgh School of Medicine, 4401 Penn Avenue, Rangos Research Center 9125, Pittsburgh, Pennsylvania 15224, USA. Phone: 412.692.7767; Fax: 412.692.7636; E-mail: Shabaana.Khader@chp.edu.

1. Dye C, Scheele S, Dolin P, Pathania V, Raviglione M. Global burden of tuberculosis. Estimated incidence, prevalence, and mortality by country. *JAMA*. 1999;282:677–686.
2. Saunders BM, Cooper AM. Restraining mycobacteria: role of granulomas in mycobacterial infections. *Immunol Cell Biol*. 2000;78(4):334–341.
3. Ulrichs T, et al. Human tuberculous granulomas induce peripheral lymphoid follicle-like structures to orchestrate local host defence in the lung. *J Pathol*. 2004;204(2):217–228.
4. Phuah JY, Mattila JT, Lin PL, Flynn JL. Activated B cells in the granulomas of nonhuman primates infected with Mycobacterium tuberculosis. *Am J Pathol*. 2012;181(2):508–514.
5. Carragher DM, Rangel-Moreno J, Randall TD. Ectopic lymphoid tissues and local immunity. *Semin Immunol*. 2008;20(1):26–42.
6. Moyron-Quiroz JE, et al. Role of inducible bronchus associated lymphoid tissue (iBALT) in respiratory immunity. *Nat Med*. 2004;10(9):927–934.
7. Tsai MC, et al. Characterization of the tuberculous granuloma in murine and human lungs: cellular composition and relative tissue oxygen tension. *Cell Microbiol*. 2006;8(2):218–232.
8. Ulrichs T, et al. Differential organization of the local immune response in patients with active cavitary tuberculosis or with nonprogressive tuberculoma. *J Infect Dis*. 2005;192(1):89–97.
9. Vinuesa CG, Tangye SG, Moser B, Mackay CR. Follicular B helper T cells in antibody responses and autoimmunity. *Nat Rev Immunol*. 2005;5(11):853–865.
10. Haynes NM, Allen CD, Lesley R, Ansel KM, Killeen N, Cyster JG. Role of CXCR5 and CCR7 in follicular Th cell positioning and appearance of a programmed cell death gene-1high germinal center-associated subpopulation. *J Immunol*. 2007; 179(8):5099–5108.
11. Yu D, et al. The transcriptional repressor Bcl-6 directs T follicular helper cell lineage commitment. *Immunity*. 2009;31(3):457–468.
12. Johnston RJ, et al. Bcl6 and Blimp-1 are reciprocal and antagonistic regulators of T follicular helper cell differentiation. *Science*. 2009;325(5943):1006–1010.
13. Nurieva RI, et al. Bcl6 mediates the development of T follicular helper cells. *Science*. 2009; 325(5943):1001–1005.
14. Junt T, et al. CXCR5-dependent seeding of follicular niches by B and Th cells augments antiviral B cell responses. *J Immunol*. 2005;175(11):7109–7116.
15. Spolski R, Leonard WJ. Interleukin-21: basic biology and implications for cancer and autoimmunity. *Annu Rev Immunol*. 2008;26:57–79.
16. Gunn MD, Ngo VN, Ansel KM, Ekland EH, Cyster JG, Williams LT. A B-cell-homing chemokine made in lymphoid follicles activates Burkitt's lymphoma receptor-1. *Nature*. 1998;391(6669):799–803.
17. Ansel KM, McHeyzer-Williams LJ, Ngo VN, McHeyzer-Williams MG, Cyster JG. In vivo-activated CD4 T cells upregulate CXC chemokine receptor 5 and reprogram their response to lymphoid chemokines. *J Exp Med*. 1999;190(8):1123–1134.
18. Kahnert A, Hopken UE, Stein M, Bandermann S, Lipp M, Kaufmann SH. Mycobacterium tuberculosis triggers formation of lymphoid structure in murine lungs. *J Infect Dis*. 2007;195(1):46–54.
19. Khader SA, et al. In a murine tuberculosis model, the absence of homeostatic chemokines delays granuloma formation and protective immunity. *J Immunol*. 2009;183(12):8004–8014.
20. Day TA, et al. Secondary lymphoid organs are dispensable for the development of T-cell-mediated immunity during tuberculosis. *Eur J Immunol*. 2010; 40(6):1663–1673.
21. Rangel-Moreno J, et al. The development of inducible bronchus-associated lymphoid tissue depends on IL-17. *Nat Immunol*. 2011;12(7):639–646.
22. Cooper AM, Khader SA. The role of cytokines in the initiation, expansion, and control of cellular immunity to tuberculosis. *Immunol Rev*. 2008; 226:191–204.
23. Casanova JL, Abel L. Genetic dissection of immunity to mycobacteria: the human model. *Annu Rev Immunol*. 2002;20:581–620.
24. Flynn JL, et al. Tumor necrosis factor-alpha is required in the protective immune response against *Mycobacterium tuberculosis* in mice. *Immunity*. 1995;2(6):561–572.
25. Rangel-Moreno J, Hartson L, Navarro C, Gaxiola M, Selman M, Randall T. Inducible bronchus-associated lymphoid tissue (iBALT) in patients with pulmonary complications of rheumatoid arthritis. *J Clin Invest*. 2006;116(12):3183–3194.
26. Mehra S, et al. Reactivation of latent tuberculosis in rhesus macaques by co-infection with Simian Immunodeficiency Virus. *J Med Primatol*. 2011;40(4):233–243.
27. Flynn JL, Chan J, Lin PL. Macrophages and control of granulomatous inflammation in tuberculosis. *Mucosal Immunol*. 2011;4(3):271–278.
28. Kang DD, Lin Y, Moreno JR, Randall TD, Khader SA. Profiling early lung immune responses in the mouse model of tuberculosis. *PLoS One*. 2011;6(1):e16161.
29. Turner J, Frank AA, Brooks JV, Gonzalez-Juarrero M, Orme IM. The progression of chronic tuberculosis in the mouse does not require the participation of B lymphocytes or interleukin-4. *Exp Gerontol*. 2001;36(3):537–545.
30. Maglione PJ, Xu J, Chan J. B cells moderate inflammatory progression and enhance bacterial containment upon pulmonary challenge with Mycobacterium tuberculosis. *J Immunol*. 2007;178(11):7222–7234.
31. Francisco LM, Sage PT, Sharpe AH. The PD-1 pathway in tolerance and autoimmunity. *Immunol Rev*. 2010;236:219–242.
32. Seiler P, et al. Early granuloma formation after aerosol Mycobacterium tuberculosis infection is

regulated by neutrophils via CXCR3-signaling chemokines. *Eur J Immunol*. 2003;33(10):2676–2686.
33. Forster R, Mattis AE, Kremmer E, Wolf E, Brem G, Lipp M. A putative chemokine receptor, BLR1, directs B cell migration to defined lymphoid organs and specific anatomic compartments of the spleen. *Cell*. 1996;87(6):1037–1047.
34. Reiley WW, et al. ESAT-6-specific CD4 T cell responses to aerosol Mycobacterium tuberculosis infection are initiated in the mediastinal lymph nodes. *Proc Natl Acad Sci U S A*. 2008;105(31):10961–10966.
35. Bauquet AT, et al. The costimulatory molecule ICOS regulates the expression of c-Maf and IL-21 in the development of follicular T helper cells and TH-17 cells. *Nat Immunol*. 2009;10(2):167–175.
36. Nurieva RI, et al. Generation of T follicular helper cells is mediated by interleukin-21 but independent of T helper 1, 2, or 17 cell lineages. *Immunity*. 2008;29(1):138–149.
37. Vogelzang A, McGuire HM, Yu D, Sprent J, Mackay CR, King C. A fundamental role for interleukin-21 in the generation of T follicular helper cells. *Immunity*. 2008;29(1):127–137.
38. Vermi W, et al. Role of dendritic cell-derived CXCL13 in the pathogenesis of Bartonella henselae B-rich granuloma. *Blood*. 2006;107(2):454–462.
39. Carlsen HS, Baekkevold ES, Morton HC, Haraldsen G, Brandtzaeg P. Monocyte-like and mature macrophages produce CXCL13 (B cell-attracting chemokine 1) in inflammatory lesions with lymphoid neogenesis. *Blood*. 2004;104(10):3021–3027.
40. Takemura S, et al. Lymphoid neogenesis in rheumatoid synovitis. *J Immunol*. 2001;167(2):1072–1080.
41. Mazzucchelli L, et al. BCA-1 is highly expressed in Helicobacter pylori-induced mucosa-associated lymphoid tissue and gastric lymphoma. *J Clin Invest*. 1999;104(10):R49–R54.
42. Shi K, et al. Lymphoid chemokine B cell-attracting chemokine-1 (CXCL13) is expressed in germinal center of ectopic lymphoid follicles within the synovium of chronic arthritis patients. *J Immunol*. 2001; 166(1):650–655.
43. Lisignoli G, et al. Human osteoblasts express functional CXC chemokine receptors 3 and 5: activation by their ligands, CXCL10 and CXCL13, significantly induces alkaline phosphatase and beta-N-acetylhexosaminidase release. *J Cell Physiol*. 2003;194(1):71–79.
44. Rangel-Moreno J, Moyron-Quiroz JE, Hartson L, Kusser K, Randall TD. Pulmonary expression of CXC chemokine ligand 13, CC chemokine ligand 19, and CC chemokine ligand 21 is essential for local immunity to influenza. *Proc Natl Acad Sci U S A*. 2007;104(25):10577–10582.
45. Kim HS, Zhang X, Choi YS. Activation and proliferation of follicular dendritic cell-like cells by activated T lymphocytes. *J Immunol*. 1994;153(7):2951–2961.
46. Lindhout E, van Eijk M, van Pel M, Lindeman J, Dinant HJ, de Groot C. Fibroblast-like synoviocytes from rheumatoid arthritis patients have intrinsic properties of follicular dendritic cells. *J Immunol*. 1999;162(10):5949–5956.
47. Lee IY, Choe J. Human follicular dendritic cells and fibroblasts share the 3C8 antigen. *Biochem Biophys Res Commun*. 2003;304(4):701–707.
48. Fazilleau N, McHeyzer-Williams LJ, Rosen H, McHeyzer-Williams MG. The function of follicular helper T cells is regulated by the strength of T cell antigen receptor binding. *Nat Immunol*. 2009; 10(4):375–384.
49. Reinhardt RL, Liang HE, Locksley RM. Cytokine-secreting follicular T cells shape the antibody repertoire. *Nat Immunol*. 2009;10(4):385–393.
50. King IL, Mohrs M. IL-4-producing CD4+ T cells in reactive lymph nodes during helminth infection are T follicular helper cells. *J Exp Med*. 2009; 206(5):1001–1007.
51. Zaretsky AG, Taylor JJ, King IL, Marshall FA, Mohrs M, Pearce EJ. T follicular helper cells differentiate from Th2 cells in response to helminth antigens. *J Exp Med*. 2009;206(5):991–999.
52. Nakayamada S, et al. Early Th1 cell differentiation is marked by a Tfh cell-like transition. *Immunity*. 2011;35(6):919–931.
53. Lu KT, et al. Functional and epigenetic studies reveal multistep differentiation and plasticity of in vitro-generated and in vivo-derived follicular T helper cells. *Immunity*. 2011;35(4):622–632.
54. Gallegos AM, van Heijst JW, Samstein M, Su X, Pamer EG, Glickman MS. A gamma interferon independent mechanism of CD4 T cell mediated control of M. tuberculosis infection in vivo. *PLoS Pathog*. 2011;7(5):e1002052.
55. Algood HM, Flynn JL. CCR5-deficient mice control Mycobacterium tuberculosis infection despite increased pulmonary lymphocytic infiltration. *J Immunol*. 2004;173(5):3287–3296.
56. Scott H, Flynn J. Mycobacterium tuberculosis in chemokine receptor 2-deficient mice: influence of dose on disease progression. *Infect Immun*. 2002;70(11):5946–5954.
57. Maglione PJ, Xu J, Casadevall A, Chan J. Fc gamma receptors regulate immune activation and susceptibility during Mycobacterium tuberculosis infection. *J Immunol*. 2008;180(5):3329–3338.
58. Mehra S, et al. The Mycobacterium tuberculosis stress response factor SigH is required for bacterial burden as well as immunopathology in primate lungs. *J Infect Dis*. 2012;205(8):1203–1213.
59. Roberts A, Cooper A, Belisle J, Turner J, Gonzalez-Juarerro M, Orme I. Murine models of tuberculosis. In: Kaufmann S, Kabelitz D, eds. *Methods in Microbiology*. London, United Kingdom: Academic Press; 2002:433–462.
60. Khader SA, et al. IL-23 and IL-17 in the establishment of protective pulmonary CD4+ T cell responses after vaccination and during Mycobacterium tuberculosis challenge. *Nat Immunol*. 2007;8(4):369–377.
61. Aujla SJ, et al. IL-22 mediates mucosal host defense against Gram-negative bacterial pneumonia. *Nat Med*. 2008;14(3):275–281.
62. Fallert BA, Reinhart TA. Improved detection of simian immunodeficiency virus RNA by in situ hybridization in fixed tissue sections: combined effects of temperatures for tissue fixation and probe hybridization. *J Virol Methods*. 2002;99(1–2):23–32.
63. Khader SA, et al. Interleukin 12p40 is required for dendritic cell migration and T cell priming after Mycobacterium tuberculosis infection. *J Exp Med*. 2006;203(7):1805–1815.
64. Lin Y, et al. Interleukin-17 is required for T helper 1 cell immunity and host resistance to the intracellular pathogen francisella tularensis. *Immunity*. 2009;31(5):799–810.
65. You Y, Richer EJ, Huang T, Brody SL. Growth and differentiation of mouse tracheal epithelial cells: selection of a proliferative population. *Am J Physiol Lung Cell Mol Physiol*. 2002;283(6):L1315–L1321.